Journal of Structural Geology, Vol. 15, No. 7, pp. 865 to 885, 1993
Printed in Great Britain

0191-8141/93 $06.00+0.00

Competence contrasts in ductile deformation as illustrated from naturally deformed chert–mudstone layers

KYUICHI KANAGAWA

Department of Geology, University of Tokyo, Tokyo 113, Japan

(*Received* 10 *March* 1992; *accepted in revised form* 25 *August* 1992)

Abstract—A sample of chert–mudstone layers provides a rare opportunity for quantitative analyses of competence contrasts in naturally deformed rocks. This sample contains deformed quartz veins, possibly formed subperpendicular to bedding during initial bedding–normal compaction, and abundant radiolarians as strain markers whose viscosity during deformation is approximated by that of chert. Under several assumptions these allow quantitative analyses of two types of competence contrast in ductile deformation, layer competence contrast and inclusion/matrix competence contrast. Layer competence contrast results in strain and cleavage refraction through the layers, while inclusion/matrix competence contrast is illustrated by the difference in strain state between radiolarians and their matrix. A quartz vein presumed to be initially perpendicular to bedding provides estimates of layer-parallel shear strains and chert/mudstone layer viscosity ratios which were also used as radiolaria/matrix viscosity ratios in different layers. Radiolarian shapes are factorized into cleavage strains and pre-cleavage shapes. Cleavage strains in matrix are then determined from radiolarian strains applying Eshelby's equations, and their variations as well as the refraction of cleavage through the layers are compared with Treagus's theoretical modeling of strain refraction.

With decreasing layer competence, cleavage refracts toward bedding and increases in intensity so that cleavage–bedding intersections vary slightly but systematically through the layers, suggesting a three-dimensional strain refraction. All three principal axes of radiolarian and matrix cleavage strain ellipsoids estimated indeed refract from layer to layer. Strain magnitude systematically increases with decreasing layer competence. These results are consistent with the strain refraction theory. However, no systematic change in strain ellipsoid shape associated with strain refraction is recognized.

INTRODUCTION

Two different terms, *competence* and *ductility*, are commonly used to describe the variation in rock properties during deformation. These are distinguished by Hobbs *et al.* (1976, pp. 67–68) and Means (1990) so that competence denotes a relative brittle or ductile strength while ductility measures the ability to undergo permanent strain without failure, although we often use the term 'competence' loosely as a measure of inverse relative ductility (e.g. Ramsay 1982).

Competence in ductile deformation therefore refers to the flow strength which is given by such parameters as differential stress at constant strain-rate or strain-rate at constant differential stress, and thus depends on the rheology of flowing rocks. Flow strength in Newtonian rheology is directly related with viscosity which is a material constant, while it can be also related in non-Newtonian rheology with effective viscosity which is not a material constant in this case and will vary in time and space (Treagus & Sokoutis 1992). In this paper *competence contrast* in ductile deformation is used to describe effective viscosity ratios in rocks, as in Treagus (1988).

Two types of competence contrast affect ductile deformation; layer competence contrast and inclusion/matrix competence contrast. The influences of layer competence contrasts in rocks are seen as variations in dominant fold wavelengths and shapes of folds and boudins, and also as strain and cleavage refractions, while those of inclusion/matrix competence contrasts recognized as variations in finite strain state between are inclusions and matrix (e.g. Ramsay 1982).

Cleavage refraction in layers of differing lithology has been described since Sorby (1853) and Harker (1886) who already considered this phenomenon as a refraction of strain. If it can be assumed that cleavage forms parallel to the XY plane of the finite strain ellipsoid and develops according to strain magnitude, refracting cleavage demonstrates the changing orientations and magnitudes of finite strains (Ramsay 1982, Ramsay & Huber 1983, p. 184, 1987, p. 462). Theoretical aspects of stress and strain refraction across layers of different viscosities have been studied in detail by Treagus (1973, 1981, 1983, 1988). She assumed planar Newtonian layers with perfect adherence and derived an important rule that the ratio of layer-parallel finite shear strains in adjacent layers is equal to the inverse of their viscosity ratio (Treagus 1983, also Cobbold 1983, Weijermars 1992), which was recently confirmed for the case of layer-parallel simple shear by model experiments (Treagus & Sokoutis 1992). She showed that finite strains should, in theory, strongly vary in magnitude, ellipsoid shape and orientation across viscosity contrasts (Treagus 1983, 1988). For cleavage subparallel to finite XY planes, cleavage–bedding intersections would vary in orientation across layers if all three principal strain axes are oblique to layering (Treagus 1988). Other geological implications of strain and cleavage refraction in rocks are discussed by Treagus (1983, 1988). However, virtually no example of quantitative analysis of strain and cleavage refraction in naturally deformed rocks has been reported so far.

Inclusion/matrix competence contrasts result in variations in finite strain state between inclusions and matrix as well as between inclusions of contrasting competences (Ramsay 1982, Lisle 1985, pp. 23–25). This has been illustrated with pebbles in conglomerates or oolites in limestones (e.g. Gay 1968b, 1969, Tan 1974, Gay & Fripp 1976, Lisle & Savage 1982, Lisle *et al.* 1983, Ramsay & Huber 1983, pp. 107–109, Freeman & Lisle 1987), and also experimentally (Gay 1968a, Tan 1974, Gay & Jaeger 1975). Gay (1968a) developed a two-dimensional theory on deformation of Newtonian viscous inclusions in a matrix of contrasting viscosity by pure and simple shears, and attempted to extend his theory to three dimensions where strain only differs in magnitude between an initially spherical inclusion and its matrix. But the equations derived by Gay (1968a) were pointed out to be incorrect by Bilby *et al.* (1975), who extended Eshelby's (1957) theory on linear elastic deformation of an ellipsoidal inclusion with different elastic constants from those of matrix, to slow incompressible Newtonian flow of a viscous inclusion embedded in a matrix of contrasting viscosity, using the well-known analogy between these two types of deformation. They applied this theory to special irrotational deformations of an elliptic cylinder and of uniaxially prolate and oblate ellipsoids. Eshelby's (1957) equations have been solved numerically for two-dimensional pure and simple shears of an arbitrary elliptic cylinder by Bilby & Kolbuszewski (1977) and for three-dimensional irrotational deformation of an arbitrary ellipsoid by Freeman (1987). Freeman (1987) predicted that strain differs not only in magnitude but also in ellipsoid shape between an inclusion and its matrix. A competent inclusion embedded in an incompetent matrix thus deforms to a more prolate shape than the matrix strain ellipsoid, which was supported by data from naturally deformed conglomerates (Freeman & Lisle 1987). Applications of these two- and three-dimensional solutions of Eshelby's (1957) equations to naturally deformed rocks are, however, still rare (Lisle *et al.* 1983, Freeman & Lisle 1987).

The purpose of this paper is to present tentative quantitative analyses of these two types of competence contrasts and to test Treagus's theoretical modeling of strain refraction in naturally deformed rocks. A sample of chert–mudstone layers with refracted cleavage contains deformed quartz veins possibly formed subperpendicular to bedding during initial bedding–normal compaction and abundant radiolarians as strain markers whose viscosity during deformation is approximated by that of chert. Cleavage orientation measurement on two sections reveals a refraction of cleavage through the layers. A quartz vein presumed to be initially perpendicular to bedding provides estimates of layer-parallel shear strains. Axial ratios and orientations of radiolarians from three sets of sections allow factorizing two- and three-dimensional radiolarian shapes into components of pre-cleavage shapes and cleavage strains. Cleavage strains in the matrix are then determined from radiolarian strains applying Eshelby's equations. This sample therefore allows the first quantification of strain and cleavage refraction in naturally deformed rocks and provides a test for Treagus's theoretical modeling of strain refraction. These analyses are, however, made possible under several assumptions whose validities as well as the limitations of the analyses are also discussed.

SAMPLE DESCRIPTION

The sample analyzed in this study was collected from a Permian–Triassic chert formation in Kawai area of the central Kitakami Mountains, where cleavage deformation took place during Early Cretaceous time under greenschist facies conditions (cf. Kanagawa 1991). This sample consists of a 1 cm thick purple chert layer, which exhibits pinch-and-swell structure, embedded in dark purple mudstone (Fig. 1a).

Cleavage is well developed in the mudstone, while it is only weakly developed in the chert (Fig. 2). There is apparently another foliation characterized by alignment of phyllosilicates subparallel to bedding, which is overprinted by cleavage oblique to bedding (Fig. 1c). Because the change in lithology from chert to mudstone is gradual on both sides of the chert layer, cleavage refracts continuously through the layers as seen on a section subnormal to cleavage–bedding intersections (Fig. 2a). Quartz veins on this section also refract concomitantly with cleavage (Fig. 1b). Some quartz veins are folded and locally cut by cleavage, indicating pre- or syn-cleavage formation of these veins (Figs. 1b and 2a). Veins post-dating cleavage are also present in the sample. They are undeformed cutting clearly both cleavage and deformed veins, but they also slightly refract across layers. The refraction of these undeformed veins may be related to stress refraction (Treagus 1988). In contrast, cleavage and veins apparently do not refract on a section subparallel to cleavage–beding intersections (Fig. 2b). Cleavage traces are subparallel to bedding here, while some deformed veins are subperpendicular to bedding (Fig. 1d).

The sample contains abundant deformed radiolarians in both chert and mudstone which are used as strain markers (Fig. 2). Many radiolarians apparently have their long axes oriented close to bedding rather than cleavage (Fig. 1c). An initial preferred orientation of radiolarians parallel to bedding is also implied by radiolarian R_f/ϕ data distributions and θ-distribution tests (e.g. Figs. 4a–c). These as well as the bedding-parallel foliation suggest the existence of a bedding-parallel pre-cleavage fabric.

ANALYTICAL PROCEDURES

Sample preparation

Specimen co-ordinates are chosen here such that the x axis is parallel to an approximate direction of cleavage–bedding intersections and the z axis normal to bedding (Fig. 3a). The mudstone on each side of the chert layer

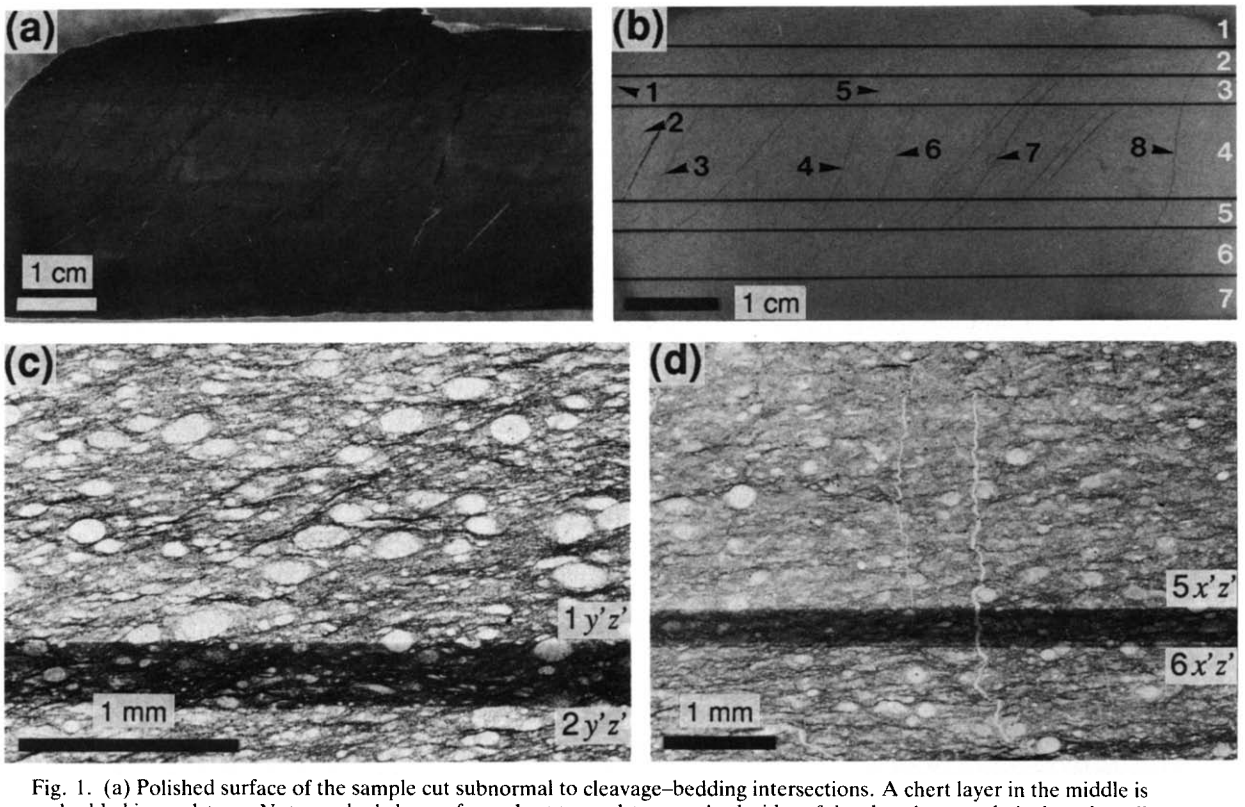

Fig. 1. (a) Polished surface of the sample cut subnormal to cleavage–bedding intersections. A chert layer in the middle is embedded in mudstone. Note gradual change from chert to mudstone on both sides of the chert layer and pinch-and-swell structure of the chert layer. (b) $y'z'$ section showing refraction of quartz veins. Domain bondaries are shown (horizontal). White numbers (1–7) indicate layers, while black numbers (1–8) with arrowheads indicate deformed quartz veins whose orientations were measured. Note folded deformed veins. Deformed veins as well as undeformed veins refract through layers. (c) Optical micrograph in plane light of an area on the $y'z'$ section. $1y'z'$ and $2y'z'$ indicate domains. Bedding trace is horizontal. Cleavage traces run from upper right to bottom left. Note a foliation subparallel to bedding and radiolarians whose long axes preferentially lie between cleavage and bedding. (d) Optical micrograph in plane light of an area on the $x'z'$ section. $5x'z'$ and $6x'z'$ indicate domains. Bedding trace is horizontal. Note that both cleavage and radiolarian long axes are subparallel to bedding, and also that folded quartz veins (center) are subperpendicular to bedding. See Fig. 3 and text for definition of layers, sections and domains.

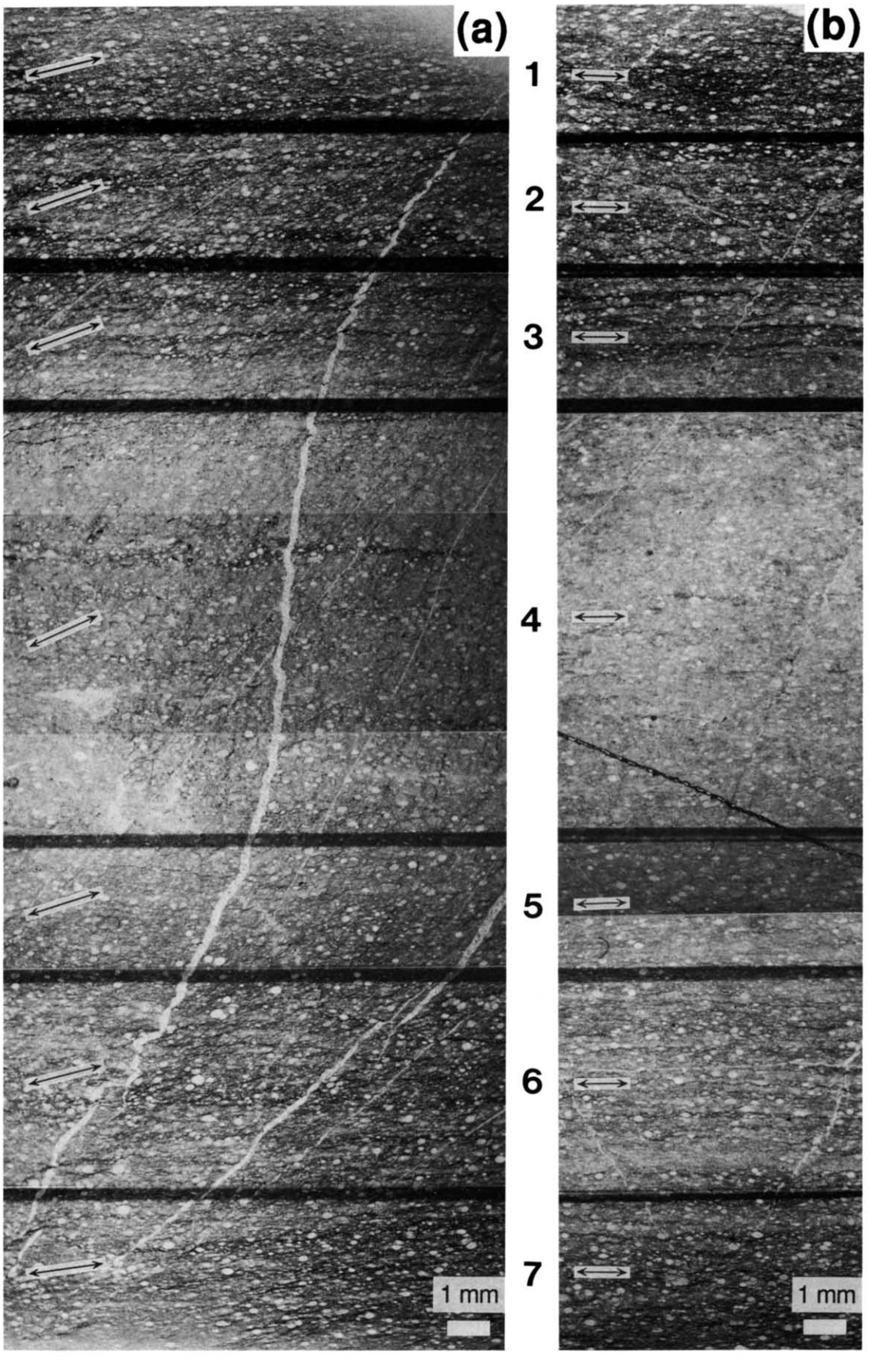

Fig. 2. Optical micrographs in plane light showing traverses across all domains on the $y'z'$ (a) and $x'z'$ (b) sections. See Fig. 3 for sections and domains. Numbers indicate layers. Bedding trace is horizontal. Lines with arrowheads mark the average cleavage directions in domains. (a) Note that cleavage, radiolarian long axes and quartz veins all refract through layers. A deformed quartz vein in center (vein 8 in Fig. 1b) is asymmetrically folded and locally cut by cleavage. (b) Note that cleavage and radiolarian long axes remain subparallel to bedding, and that quartz veins do not refract on this section.

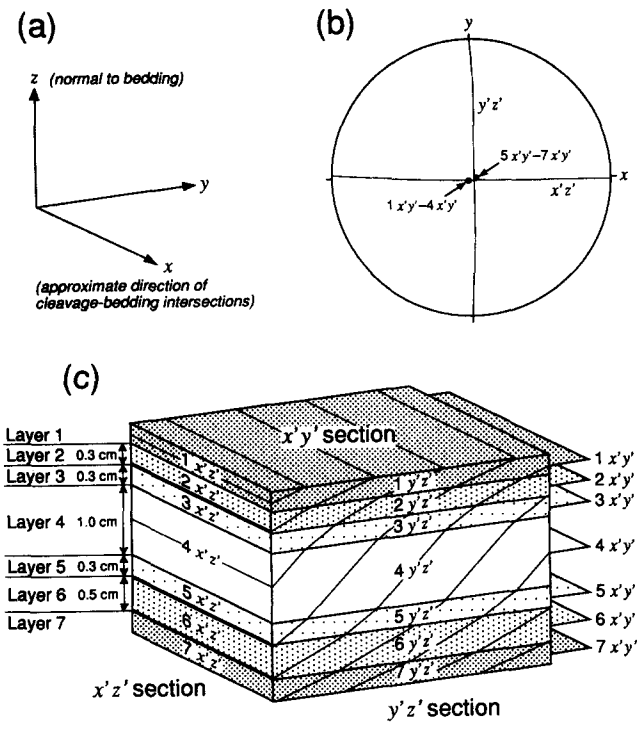

Fig. 3. (a) Specimen co-ordinates with reference to bedding and cleavage used in this study. (b) Orientations of the $x'y'$, $y'z'$ and $x'z'$ sections. Equal-area lower-hemisphere projection. π-poles of $x'y'$ sections and great circles of $y'z'$ and $x'z'$ sections are shown. (c) Schematic block diagram illustrating seven layers, three groups of sections, and seven domains on each section. Layer 4 is the chert layer. Cleavage traces on three different sections are also schematically shown. Their orientations are arbitrarily exaggerated.

was arbitrarily divided into three layers of 0.3–0.5 cm thickness so that the sample is composed of one chert layer and six mudstone layers. These layers are labeled as layers 1–7, the chert layer being layer 4 (Fig. 3c). Two approximately orthogonal sections were cut from the sample for analysis. One is subnormal to cleavage–bedding intersections ($y'z'$ section), and the other subnormal to bedding and subparallel to cleavage–bedding intersections ($x'z'$ section) (Figs. 3b & c). Every layer has a cut surface area on each section, which is called here a domain. Domains are labeled as $1y'z'$–$7y'z'$ on the $y'z'$ section, and as $1x'z'$–$7x'z'$ on the $x'z'$ section (Fig. 3c, e.g. Figs. 1b & c). A third set of sections were cut subparallel to bedding from the middle of every layer, and are labeled as $1x'y'$–$7x'y'$ (Figs. 3b & c).

Cleavage orientation measurement

Orientations of at least 200 cleavage traces in every domain on both $y'z'$ and $x'z'$ sections were measured under the microscope, using the convention that anticlockwise orientations from the bedding trace direction are positive. The vector mean direction of cleavage trace measurements was then calculated and used as an average cleavage direction in each domain. The average cleavage plane in each layer was determined from the two vector mean directions derived for the domains on $y'z'$ and $x'z'$ sections.

It is assumed in this study that this average cleavage plane is parallel to the finite XY plane of cleavage strain in each layer. Although the relationship between strain and cleavage is still not fully understood (see Treagus 1983 for a concise review), cleavage is apparently parallel to finite XY planes in most cases (cf. Ramsay & Huber 1983, pp. 181–184, Price & Cosgrove 1990, pp. 450–453) and also in the Kitakami slates (Kanagawa 1991).

Orientation of deformed quartz veins

Orientations of eight deformed quartz veins (1–8) on the $y'z'$ section (Fig. 1b) were measured (Table 1). In each domain, the direction of a line joining two intercepts of a vein with the domain boundaries was taken as the mean orientation of that vein. More strongly folded and cleaved veins (veins 2, 4 and 8) record larger strains than less deformed veins, thus probably formed in an early stage pre-dating cleavage, possibly subperpendicular to bedding during initial bedding-normal compaction. Among these veins, vein 8 (Figs. 1b and 2a) was selected as a reference and assumed to be initially perpendicular to bedding, because this is the only vein extending through all layers.

Initial bedding-normal compaction is suggested by bedding-parallel foliation as well as initial preferred orientation of radiolarians. This compaction is expected to have produced quartz veins perpendicular to bedding, as preserved in a section subparallel to cleavage–bedding intersections (Fig. 1d).

Two-dimensional strain analysis using a deformed quartz vein

If vein 8 was perpendicular to bedding before cleavage development, the present orientation of this quartz vein provides an estimate of layer-parallel finite shear strain during the cleavage deformation. Layer-parallel, angular shear and shear strain (ψ and γ) are thus calculated through the layers.

Because the trace of finite XY plane on any section is not generally parallel to the long axis of strain ellipse in that section (cf. Ramsay 1967, p. 160), cleavage traces on the $y'z'$ section do not necessarily indicate the orientation of cleavage strain ellipse in this section even if cleavage is parallel to the finite XY plane of cleavage strain. However, since the $y'z'$ section is subperpendicular to cleavage for all layers, the angular difference between the cleavage trace and the long axis of cleavage strain ellipse would be negligible in all layers in this section. The average cleavage direction in each domain on the $y'z'$ section is thus regarded parallel to the long axis of cleavage strain ellipse. Knowing the orientation of strain ellipse and one measurement of angular shear in any direction, we can calculate the strain ratio (Ramsay & Huber 1983, pp. 128–130). In this case, the strain-ellipse orientation is taken as the average cleavage direction, and the angular shear in the bedding direction (ψ) is known from the orientation of the reference vein. The strain ratio (R_s) for each layer in the $y'z'$ section is

Table 1. Orientations of eight deformed quartz veins (1–8 in Fig. 1b) on the $y'z'$ section. Orientations are measured positive anticlockwise from bedding trace direction

	Vein 1	Vein 2	Vein 3	Vein 4	Vein 5	Vein 6	Vein 7	Vein 8
Layer 1	47.5	—	39.5	—	47.0	39.5	—	48.0
Layer 2	51.5	62.0	38.5	—	55.0	48.0	38.5	54.0
Layer 3	59.5	69.0	51.0	—	59.0	51.5	46.0	68.0
Layer 4	74.0	72.0	60.0	70.0	—	65.5	55.0	81.0
Layer 5	—	—	44.5	54.5	—	45.0	46.0	64.0
Layer 6	—	—	—	49.5	—	42.0	39.0	56.0
Layer 7	—	—	—	48.0	—	—	—	52.5

therefore calculated using equation (8.18) of Ramsay & Huber (1983, p. 141):

$$R_s^2 = \frac{\tan \psi + \tan \phi}{\tan \phi - \tan^2 \phi \tan \psi},$$

where ϕ is the angle between cleavage and bedding in a domain.

If the quartz vein was exactly perpendicular to initial bedding, the strain ratio thus determined for each layer would give a precise estimate of mean bulk strain ratio during cleavage development, and can be used for comparison with the cleavage strain in the matrix derived from radiolarians. However, since R_s is a function of tan ψ, a small deviation of the vein orientation from bedding-perpendicular would result in large errors in strain ratios.

Estimation of effective viscosity ratios

Assuming that the ratio of layer-parallel shear strains is the inverse of layer viscosity ratio, the effective viscosity ratio of layer i with respect to layer 4 (chert) during cleavage development is calculated using the following equation:

$$\frac{\mu_i}{\mu_4} = \frac{\gamma_4}{\gamma_i},$$

where γ_i, μ_i, γ_4, μ_4 are layer-parallel shear strain and effective viscosity in layer i and layer 4, respectively.

This assumption holds for Newtonian layers with coherent interfaces (Cobbold 1983, Treagus 1983). On a coherent interface in Newtonian layers, the layer-parallel shear stress should be equal in adjoining layers so that the ratio of layer-parallel shear strain rate, and hence of layer-parallel shear strain in this case, is the inverse of layer viscosity ratio. The chert–mudstone layer boundaries in the sample analyzed are considered to have been coherent, because the lithology gradually changes and no sign of slip along these boundaries is recognized. Microstructures in this sample indicate syntectonic crystallization–recrystallization of phyllosilicates as well as pressure solution as the dominant processes for cleavage development (cf. Kanagawa 1991), and suggests diffusive mass transfer as the dominant deformation mechanism (cf. Knipe 1989), although radiolarians may be deformed partly by crystal plasticity. The behavior of this sample during cleavage development can therefore be approximated by a Newtonian flow, because theoretical models for diffusive mass transfer indicate a linear relationship between stress and strain-rate, i.e. Newtonian rheology (e.g. Rutter 1976, 1983, Knipe 1989, Spiers & Schutjens 1990).

Two-dimensional strain analysis using radiolarians

Radiolarians were first traced using a profile projector. Axial lengths and long-axis orientations of 10–420 radiolarians in each domain were obtained using an image analysis system described in Kanagawa (1990), and used for strain analysis. Final average radiolarian ellipses in 21 domains in three groups of sections ($x'y'$, $y'z'$ and $x'z'$) were then calculated by Wheeler's (1984) method which is equivalent with Shimamoto & Ikeda's (1976) method (details in Appendix 1; results in Table 2).

The θ-distribution tests of Peach & Lisle (1979) and Lisle (1985) were also applied to R_f/ϕ data on the $y'z'$ section where cleavage traces refract through layers.

Table 2. Final average radiolarian ellipses in domains on three groups of sections. N = number of radiolarians measured; R_f and long axis = axial ratio and long-axis orientation of final average radiolarian ellipse calculated by Wheeler's (1984) method. Plunge/azimuth angles are given as orientation data. Azimuthal angles are measured anticlockwise from the x axis

	$x'y'$ section				$y'z'$ section				$x'z'$ section			
Layer	plane normal	N	R_f	long axis	plane normal	N	R_f	long axis	plane normal	N	R_f	long axis
1	87.57/240.90	187	1.071	1.78/17.92	1.77/180.01	222	1.695	7.80/89.77	1.45/88.96	270	1.835	2.94/179.03
2	87.57/240.90	197	1.063	1.80/18.75	1.77/180.01	311	1.503	12.05/89.63	1.45/88.96	268	1.437	0.88/178.98
3	87.57/240.90	232	1.045	2.16/33.61	1.77/180.01	273	1.395	11.75/89.64	1.45/88.96	246	1.337	1.39/179.00
4	87.57/240.90	381	1.054	1.94/23.70	1.77/180.01	239	1.313	13.90/89.57	1.45/88.96	418	1.318	2.39/179.02
5	86.38/354.34	173	1.018	3.33/197.46	1.77/180.01	294	1.362	12.41/89.62	1.45/88.96	210	1.289	2.97/179.04
6	86.38/354.34	291	1.021	3.42/193.33	1.77/180.01	388	1.425	11.96/89.63	1.45/88.96	400	1.401	1.53/179.00
7	86.38/354.34	329	1.061	3.48/190.07	1.77/180.01	396	1.744	3.67/89.90	1.45/88.96	397	1.835	1.94/179.01

Although some of the seven domains passed this θ-distribution test, others failed (e.g. Fig. 4c). R_f/ϕ data of all domains have similar features such that the vector mean ϕ direction lies between the cleavage and bedding directions, that radiolarians with the highest aspect ratios are preferentially aligned around the bedding direction, and that R_f/ϕ data distributions are internally asymmetric spreading toward the bedding side (e.g. Figs. 4a & b). Such R_f/ϕ data distributions imply an initial preferred orientation of radiolarians parallel to bedding (cf. Lisle 1985, pp. 16–22), which is consistent with the observations of bedding-parallel foliation and many radiolarians with their long axes oriented close to bedding (Fig. 1c). This bedding-parallel pre-cleavage fabric is attributable to initial bedding-normal compaction which also produced quartz veins subperpendicular to bedding.

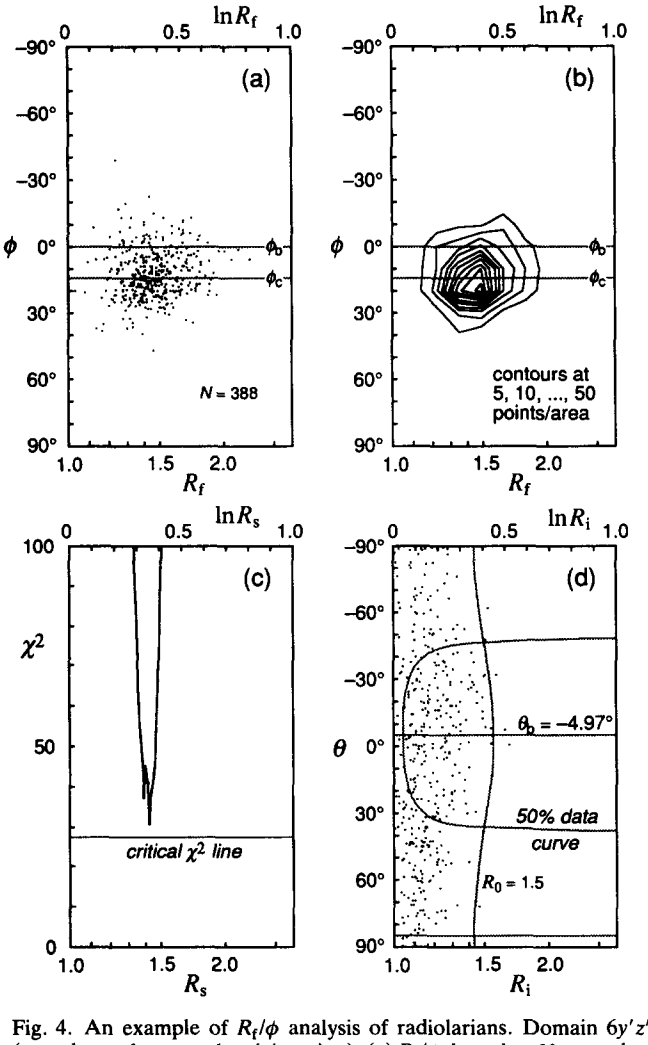

Fig. 4. An example of R_f/ϕ analysis of radiolarians. Domain 6$y'z'$ (a mudstone layer on the $y'z'$ section). (a) R_f/ϕ data plot. N = number of radiolarians measured. ϕ_b = bedding trace direction; ϕ_c = cleavage trace direction. (b) Contour map of R_f/ϕ data density. Note an internally asymmetric distribution of R_f/ϕ data as indicated by both (a) and (b). (c) Output of the θ-distribution test of Peach & Lisle (1979). Cell configurations and critical χ^2 values in θ-distribution tests are adopted from Lisle (1985). This set of R_f/ϕ data failed the θ-distribution test, and initial preferred orientation of radiolarians is implied. (d) R_i/θ plot after unstraining by a strain ratio determined by Wheeler's (1986a) method. A fitted R_i/θ curve for initial ellipticity $R_0 = 1.5$ and a 50% data curve are shown. θ_b = unstrained bedding direction.

We assume in the two-dimensional radiolarian strain analysis a pre-cleavage bedding-symmetric fabric of radiolarians in the $y'z'$ section, and a homogeneous deformation with shortening perpendicular to cleavage such that radiolarians deformed passively as their matrix. The final average radiolarian ellipse determined for each domain on the $y'z'$ section can then be factorized using Wheeler's (1986a) tensor algebraic method into a cleavage strain superimposed on an initial average radiolarian ellipse whose long axis is parallel to initial bedding (details in Appendix 1). The axial ratios of the cleavage strain ellipse and the initial average radiolarian ellipse are calculated from equations (A30) and (A31). Unstraining of radiolarian R_f/ϕ data using the radiolarian strain ratios thus obtained gives pre-cleavage radiolarian R_i/θ distributions symmetrical with initial bedding trace (e.g. Fig. 4d). It should be noted, however, that the assumption of passive deformation of radiolarians is reasonable only in the chert layer where the radiolaria/matrix competence contrast is negligible, because the competence contrasts between radiolarians and matrix in mudstone layers must have resulted in differential body rotations (cf. Gay 1968a, Freeman 1987).

In order to estimate the cleavage strains in matrix from radiolarian strains, it is further assumed that the deformation was a pure shear, and that both radiolarians and matrix were Newtonian viscous during the deformation. Radiolarian strain ellipses are therefore presumed to suffer no area change, and that their principal axes remain parallel to those of matrix strain ellipses throughout the deformation. We also assume no radiolaria/matrix competence contrast during the deformation in the chert layer, and that the viscosity of radiolaria was constant throughout the layers. The radiolaria/matrix viscosity ratio in a mudstone layer can then be considered equal to the chert/mudstone viscosity ratio already determined. Under these conditions we can calculate the matrix strain ratio for each layer from the radiolarian strain ratio using equation (A56) which is derived from Eshelby's equations according to Bilby *et al.* (1975) (details in Appendix 2). Deducing matrix cleavage strains in this way is, however, logically inconsistent with the above estimation of radiolarian strains, because the former is based on inhomogeneous deformation of radiolarians and matrix whereas the latter assumed homogeneous deformation in which radiolarians behaved passively as their matrix.

Three-dimensional strain analysis using radiolarians

Final average radiolarian ellipses on three groups of sections ($x'y'$,$y'z'$ and $x'z'$) listed in Table 2 are combined to obtain final average radiolarian ellipsoids in seven layers. Several methods giving a three-dimensional ellipsoid from two-dimensional ellipses on any three sections have been proposed (e.g. Ramsay 1967, pp. 147–149, Milton 1980, Owens 1984, De Paor 1990). Final average radiolarian ellipsoids are calculated here using Milton's (1980) method which gives ellipsoids by quadratic-form tensors **F**. The shape tensors for final

average radiolarian ellipsoids, $\mathbf{N}_f$, are then derived as $\mathbf{F}^{-1}/|\mathbf{F}^{-1}|^{1/3}$ and used for the strain analysis (see Appendix 1).

We assume in three-dimensional radiolarian strain analysis that bedding-normal compaction produced a pre-cleavage fabric such that initial average radiolarian ellipsoids are uniaxially oblate with their short axes normal to bedding. Another assumption made here is, as in two-dimensional analysis, a bulk homogeneous deformation with its finite XY plane parallel to cleavage. The final average radiolarian ellipsoid determined for each layer can then be factorized using Wheeler's (1986a) method into a cleavage strain ellipsoid and an initial average radiolarian ellipsoid of uniaxially oblate shape (details in Appendix 1). This method yields a constraint parameter ν for the input data, and the final average radiolarian ellipsoid is first corrected so as to exactly satisfy the constraint ($\nu = 0$). The squared length of bedding-parallel radius of initial average radiolarian ellipsoid is then calculated using equation (A46). Knowing this length, the shape tensors for the strain ellipsoid and the initial average radiolarian ellipsoid with its short axis normal to initial bedding are determined (Appendix 1).

In order to estimate three-dimensional cleavage strains in the matrix, we assume a constant-volume coaxial deformation such that principal strain axes of radiolarian strain ellipsoids remain parallel to those of matrix strain ellipsoids throughout the deformation, and also that both radiolarians and matrix were Newtonian viscous during the deformation. Under these assumptions and using radiolaria/matrix viscosity ratios defined above, we can calculate the matrix strain ellipsoids through the layers from radiolarian strain ellipsoids applying Eshelby's equations according to Freeman (1987) (details in Appendix 2).

RESULTS

Cleavage orientations

Orientation frequency distributions of cleavage traces in domains on $y'z'$ and $x'z'$ sections are shown in Fig. 5. In the chert layer (domains $4y'z'$ and $4x'z'$), cleavage orientations show a wide scatter and a low concentration. Fluctuation gradually decreases and concentration increases away from the chert layer, representing a gradual increase of cleavage development toward less competent layers. Peaks of orientation frequency gradually shift from domain to domain on the $y'z'$ section. Accordingly, the vector mean cleavage direction varies from 7.48° (domain $7y'z'$) to 23.86° (domain $4y'z'$) so that cleavage makes the largest angle with bedding in domain $4y'z'$ (Figs. 5a–g). This indicates a gradual refraction of cleavage through the layers as schematically shown in Fig. 7(a). In contrast, peaks and vector mean directions remain subparallel to bedding through domains on the $x'z'$ section. Both peaks and vector mean cleavage directions in this section, however, have a tendency that they slightly shift anticlockwise in more competent layers (Figs. 5h–n).

Vector mean cleavage directions on $y'z'$ and $x'z'$ sections are combined to give average cleavage planes. It should be noted that the cleavage direction on $y'z'$ section mainly affects the dip of cleavage, whereas that on $x'z'$ section the strike of cleavage (see Fig. 3). π-poles of the average cleavage planes in seven layers are shown in Fig. 6(a). A gradual refraction of cleavage through these layers is recognized. Cleavage–bedding intersections are not parallel with each other (Fig. 6b), trending ±7° from x axis. They systematically vary through the layers except layer 5 such that intersection directions rotate anticlockwise as layer competence decreases. It could be argued that such variation of cleavage–bedding intersections is fortuitous resulting from statistical errors. However, this variation mainly arises from the variation of cleavage orientations on the $x'z'$ section, which seems rather systematic (Figs. 5h–n).

Layer-parallel shear strains and effective viscosity ratios

The reference vein orientation, layer-parallel shear strains and effective viscosity ratios on the $y'z'$ section are shown in Fig. 7 and Table 3. Layer-parallel shear strain varies from 0.16 in the chert layer to 0.40–0.90 in mudstone layers (Fig. 7b). The effective viscosity ratio of mudstone/chert computed as the inverse ratio of layer-parallel shear strains gradually decreases away from the chert layer (Fig. 7c). The least competent layers (layers 1 and 7) are estimated to be about five times less viscous than the chert layer (Table 3).

Two-dimensional strains

Results of the strain analyses for the $y'z'$ section are summarized in Table 3. The final average radiolarian ellipse for each layer is factorized into an initial average radiolarian ellipse oriented parallel to initial bedding and the radiolarian cleavage strain ellipse oriented parallel to cleavage. These ellipses in seven layers are shown in Fig. 8. Figure 9 shows cleavage strain ellipses for radiolaria and matrix in seven layers. Cleavage strain ellipses in matrix are estimated by two independent methods. Matrix strain ellipses (1) are those derived from radiolarian strain ellipses applying Eshelby's equations, while matrix strain ellipses (2) are obtained from layer-parallel shear strains using the reference vein orientation.

Final average radiolarian ellipses vary in axial ratio from 1.31 (layer 4) to around 1.7 (layers 1 and 7). Their long axes always lie between cleavage and bedding directions, changing their orientations in accordance with cleavage (Fig. 8). Radiolarian cleavage strain ellipses vary in axial ratio from 1.21 (layer 4) to around 1.45 (layers 1 and 7), indicating that less competent layers record larger radiolarian strains. Their long axes are assumed parallel to average cleavage directions. Axial ratios of initial average radiolarian ellipses range from 1.05 (layer 6) to 1.24 (layer 7). They are larger in

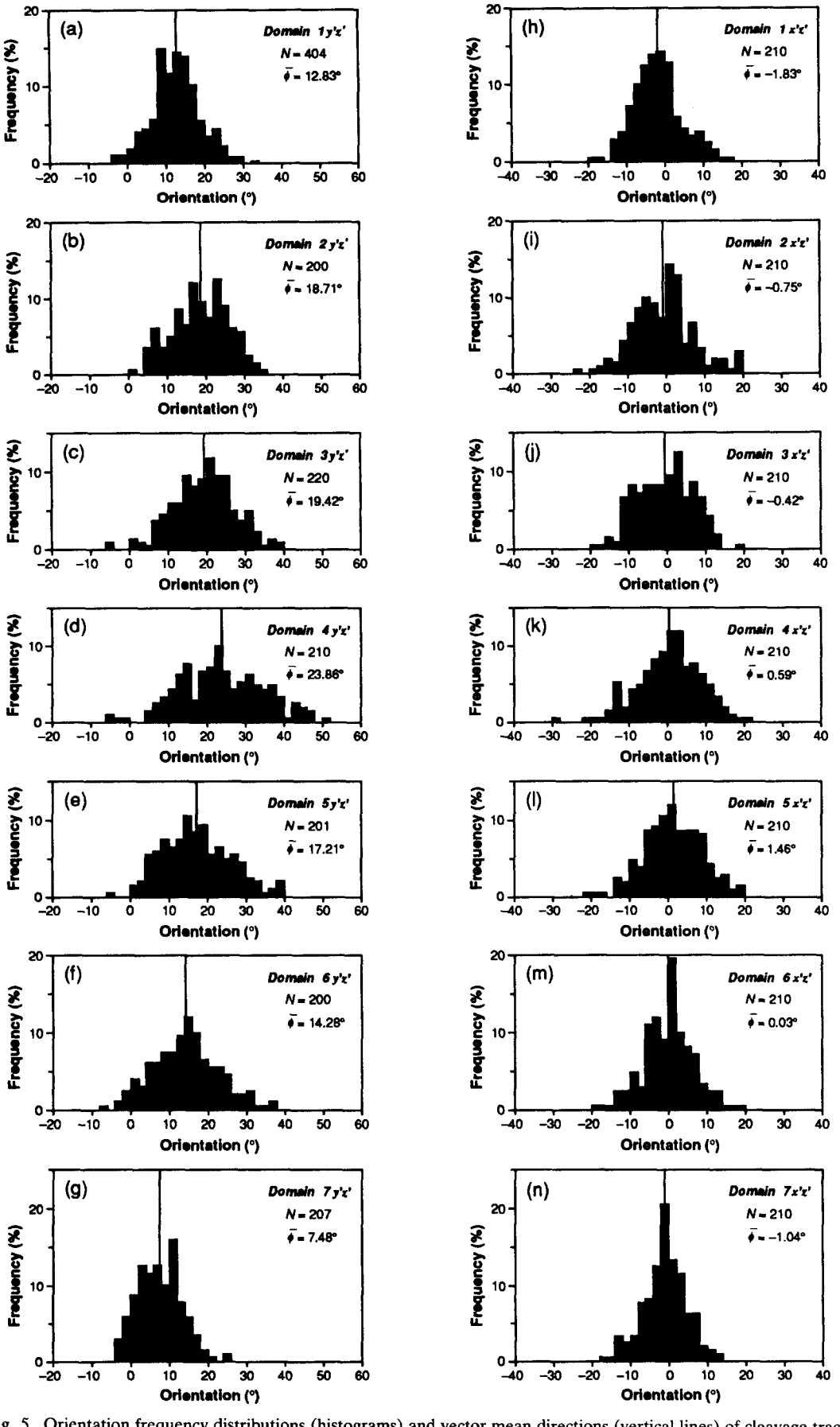

Fig. 5. Orientation frequency distributions (histograms) and vector mean directions (vertical lines) of cleavage traces in domains on $y'z'$ and $x'z'$ sections. Orientations are measured positive anticlockwise from bedding trace direction. N = number of measurements; $\bar{\phi}$ = vector mean angle.

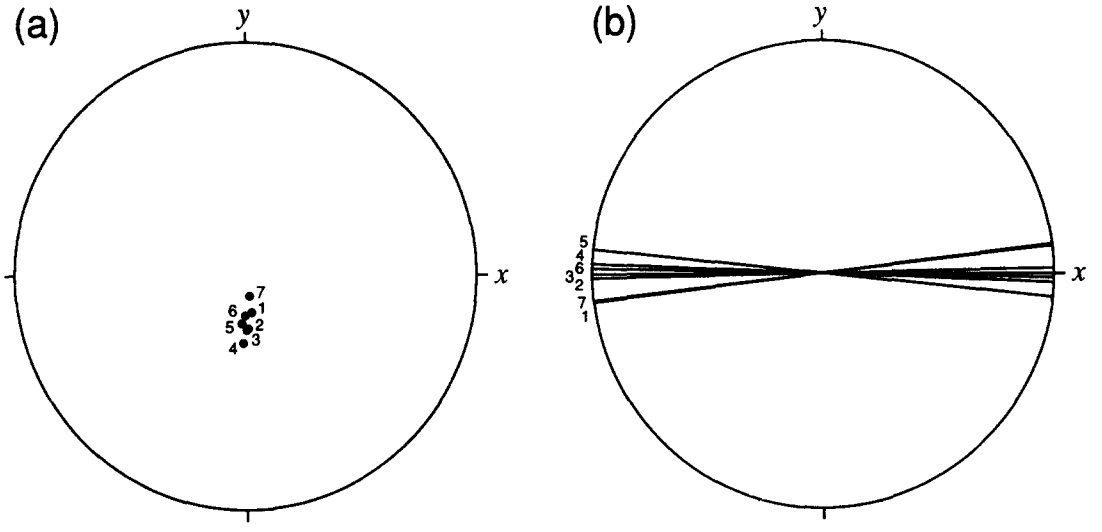

Fig. 6. Equal-area lower-hemisphere projections of cleavage (a) and cleavage–bedding intersections (b) in different layers. Numbers indicate layers. (a) π-poles of average cleavage planes. (b) Intersection directions of average cleavage planes with bedding.

layers 1 and 7, smaller in layers 5 and 6, and unchanged in layers 2–4. Initial average radiolarian ellipses have rather constant long-axis orientations ($-4.6° \pm 1.6°$) (Fig. 8 and Table 3), which correspond to initial bedding directions.

Matrix cleavage strain ratios (1) calculated from radiolarians range from 1.21 (layer 4) to 3.66 (layer 1), while those (2) calculated from layer-parallel shear strains range from 1.21 (layer 4) to 2.76 (layer 7) (Fig. 9 and Table 3). Matrix strain ratios are larger in less competent layers. It is noteworthy that both strain ratios in layer 4 (chert) exactly coincide. Matrix strain ratios (1) reasonably coincide with those (2) except in layer 1 where the former is significantly larger than the latter.

Three-dimensional strains

Data of final average radiolarian ellipsoids, corrected-final and initial average radiolarian ellipsoids, and radiolarian and matrix cleavage strain ellipsoids are shown in Tables 4–6, respectively. All ellipsoids are scaled to volume $4\pi/3$ such that $XYZ = 1$ where X, Y and Z are the principal axial lengths of ellipsoids. This is because shape tensors are used in calculating average radiolarian ellipsoids and three-dimensional strain analysis (Appendix 1). Constant-volume deformation is assumed only in deriving cleavage strain ellipsoids in the matrix. In these tables, K is the ellipsoid shape parameter after Ramsay (1967, p. 350) and $\bar{\varepsilon}_s$ is the strain magnitude parameter after Nadai (1963, pp. 50 and 73):

$$K = \frac{\ln R_{XY}}{\ln R_{YZ}}$$

$$\bar{\varepsilon}_s = \frac{1}{\sqrt{3}} \{(\ln R_{XY})^2 + (\ln R_{YZ})^2 + (\ln R_{XZ})^2\}^{1/2},$$

where R_{XY}, R_{YZ} and R_{XZ} are the principal-plane axial ratios. For radiolarian ellipsoids $\bar{\varepsilon}_s$ represents a measure of deviation from a sphere and is called here the ellipsoid strength parameter. Axes and shapes of these ellipsoids are graphically shown in Figs. 10–13.

Z axes of final average radiolarian ellipsoids slightly but systematically vary in orientation through the layers (Fig. 10a). In contrast, their X and Y axes significantly vary in orientation. Both axes, except those of layer 4, shift their azimuth directions anticlockwise toward more competent layers (Fig. 10a). The final average radiolarian ellipsoids have a narrow range of low K values (0.053–0.137) (Table 4). No systematic change in ellipsoid shape through the layers is recognized, whereas $\bar{\varepsilon}_s$ values systematically vary from 0.23 (layer 4) to 0.477 (layer 7) according to layer competence (Fig. 10b and Table 4).

Table 3. Results of strain analysis for the $y'z'$ section. $\phi_{cleavage}$ and ϕ_{vein} = orientations of cleavage and the reference vein (vein 8 in Fig. 1b); N = number of radiolarians measured; R_f and ϕ = axial ratio and long-axis orientation of final average radiolarian ellipse calculated by Wheeler's (1984) method; R_i and θ = axial ratio and long-axis orientation of initial average radiolarian ellipse resolved by Wheeler's (1986a) method; R_s^R = radiolarian cleavage strain ratio calculated by Wheeler's (1986a) method; $R_s^M(1)$ = matrix cleavage strain ratio calculated from radiolarian strain according to Bilby *et al.* (1975); ψ and γ = layer-parallel, angular shear and shear strain calculated from the reference vein; μ_i/μ_4 and μ_4/μ_i = effective viscosity ratios of layer i and layer 4 (chert); $R_s^M(2)$ = matrix cleavage strain ratio calculated from layer-parallel shear strain

Layer	$\phi_{cleavage}$	ϕ_{vein}	N	R_f	ϕ	R_i	θ	R_s^R	$R_s^M(1)$	ψ	γ	μ_i/μ_4	μ_4/μ_i	$R_s^M(2)$
1	12.83	48.0	222	1.70	7.80	1.17	−5.79	1.48	3.66	42.0	0.90	0.18	5.68	2.50
2	18.71	54.0	311	1.50	12.06	1.13	−6.17	1.37	2.40	36.0	0.73	0.22	4.59	2.04
3	19.42	68.0	273	1.40	11.76	1.12	−4.74	1.27	1.53	22.0	0.40	0.39	2.55	1.58
4	23.86	81.0	239	1.31	13.91	1.12	−4.36	1.21	1.21	9.0	0.19	1.00	1.00	1.21
5	17.21	64.0	294	1.36	12.42	1.08	−4.46	1.28	1.66	26.0	0.49	0.32	3.08	1.74
6	14.28	56.0	388	1.43	11.97	1.05	−4.97	1.37	2.29	34.0	0.67	0.23	4.26	2.10
7	7.48	52.5	396	1.74	3.67	1.24	−3.09	1.42	2.77	37.5	0.77	0.21	4.84	2.76

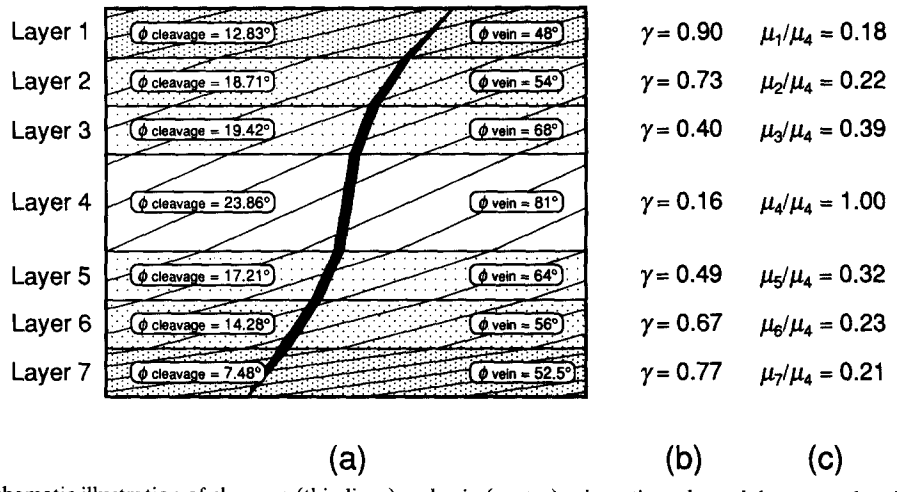

Fig. 7. (a) Schematic illustration of cleavage (thin lines) and vein (center) orientations through layers on the $y'z'$ section. Vector mean direction of cleavage traces and orientation of the reference vein (vein 8 in Fig. 1b) in each domain are shown as cleavage ($\phi_{cleavage}$) and vein (ϕ_{vein}) orientations, respectively. (b) Layer-parallel shear strains (γ) calculated from the vein orientation. (c) Effective viscosity ratios of layers with respect to the chert layer. μ_i = effective viscosity of layer i.

These final average radiolarian ellipsoids as well as average cleavage orientations through the layers yield reasonable v values ranging from -0.010 to -0.048 (Table 5). The corrected final average radiolarian ellipsoids satisfying the constraint ($v = 0$) have therefore very small difference from the corresponding uncorrected ones in both axes and shapes (Fig. 11 and Table 5).

Z axes of initial average radiolarian ellipsoids are presumed to be normal to initial bedding in all the layers and actually concentrated (Fig. 12a). X and Y axes are indeterminate because initial average radiolarian ellip-

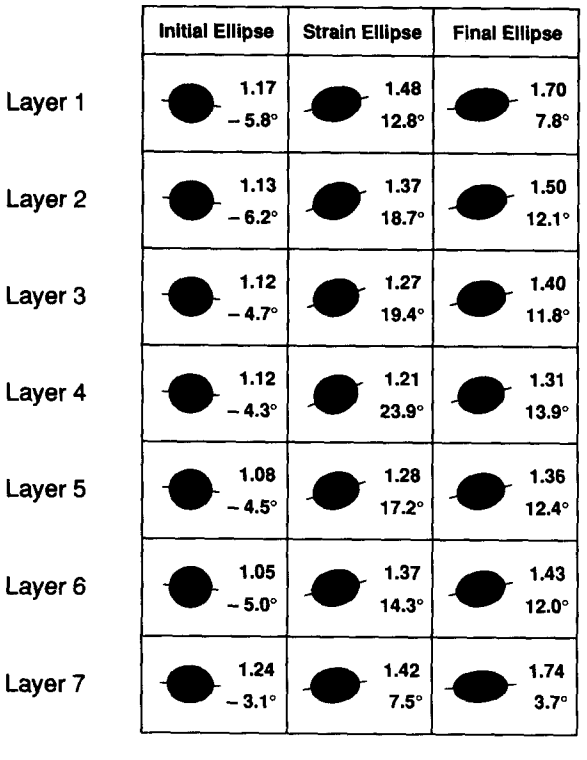

Fig. 8. Results of radiolarian strain analysis for the $y'z'$ section. Final ellipses are final average radiolarian ellipses calculated by Wheeler's (1984) method, while strain and initial ellipses are cleavage strain ellipses and initial average radiolarian ellipses factorized by Wheeler's (1986a) method. Axial ratio and long-axis orientation are indicated on the right of each ellipse. Orientations are shown positive anticlockwise from bedding trace direction.

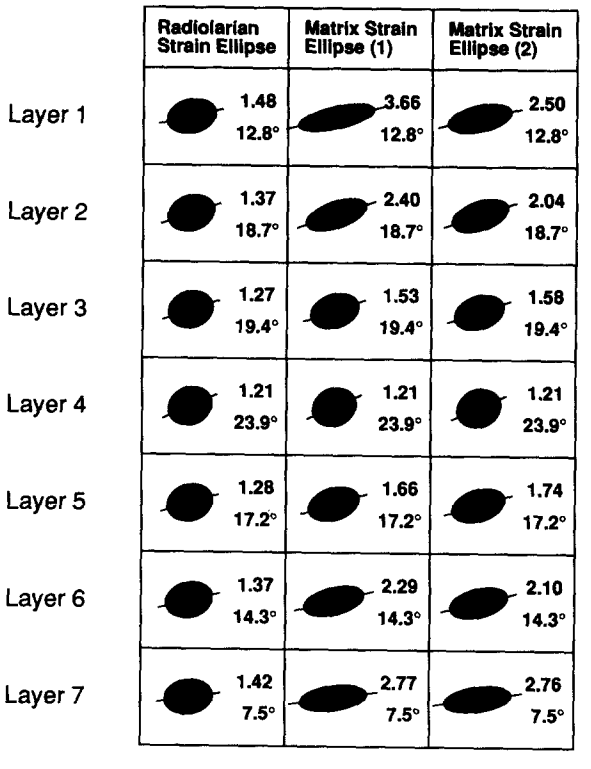

Fig. 9. Cleavage strain ellipses for radiolaria and matrix in seven layers on the $y'z'$ section. Cleavage strain ellipses in matrix are estimated by two independent methods. Matrix strain ellipses (1) are those derived from radiolarian strain ellipses according to Bilby *et al.* (1975), while matrix strain ellipses (2) are obtained from layer-parallel shear strains using the reference vein orientation. Axial ratio and long-axis orientation are indicated on the right of each ellipse. Orientations are shown positive anticlockwise from bedding trace direction.

soids are assumed to be uniaxially oblate ($K = 0$) due to pre-cleavage compaction. The $\bar{\varepsilon}_s$ values range from 0.038 (layer 6) to 0.164 (layer 7), the variation of which through layers is similar to that in axial ratios of initial average ellipses (Fig. 12b and Table 5).

The radiolarian and matrix cleavage strain ellipsoids are assumed to be coaxial, and the Z axes of the cleavage strain ellipsoids normal to average cleavage planes in different layers. Their X and Y axes significantly vary in orientation through the layers as those of final ellipsoids such that they, except those of layer 4, shift their azimuth directions anticlockwise toward competent layers (Fig. 13a). K values of radiolarian strain ellipsoids range from 0.061 (layer 6) to 0.187 (layer 3), while those of matrix strain ellipsoids from 0.058 (layer 6) to 0.183 (layer 3) (Table 6). Radiolarian strain ellipsoids are only slightly more prolate than the corresponding matrix strain ellipsoids (Fig. 13b and Table 6). There are no systematic changes through the layers for both the ellipsoid shapes (Fig. 13b). However, the strain magnitudes in both radiolarians and matrix systematically vary through layers according to layer competence. $\bar{\varepsilon}_s$ values of radiolarian strain ellipsoids range from 0.157 (layer 4) to 0.354 (layer 1), while those of matrix strain ellipsoids from 0.157 (layer 4) to 0.698 (layer 1) (Table 6). The difference in strain magnitude between radiolarians and matrix increases toward less competent layers.

DISCUSSION

Effective viscosity ratios

Effective viscosity ratios in naturally deformed rocks have been determined in two ways. Gay (1968b, 1969) estimated viscosity ratios of different rock types from deformed pebbles using his earlier derived equation (Gay 1968a). Lisle *et al.* (1983) also obtained pebble/conglomerate viscosity ratios for different pebble types using the equations after Bilby & Kolbuszewski (1977). Viscosity ratios of different rock types obtained from pebbles are commonly less than 5. Another attempt was made by Shimamoto & Hara (1976) who estimated viscosity ratios from dominant wavelength/thickness ratios of folded quartz veins in matrix schists of differing lithology using equations derived by Biot (1965a,b) and Sherwin & Chapple (1968). Viscosity ratios obtained by them range with respect to pelitic schist from ≈4 for psammitic schist, through ≈5 for mafic schist to ≈125 for quartz vein (see Treagus 1983).

The relationship derived by Cobbold (1983) and Treagus (1983) for Newtonian layers with coherent interfaces provides another simple method for estimating effective layer viscosity ratios from layer-parallel shear strains. Recent model experiments by Treagus & Sokoutis (1992) confirmed this relationship for the case of layer-

Table 4. Final average radiolarian ellipsoids calculated by Milton's (1980) method from two-dimensional section data listed in Table 2. X, Y, Z = principal axial lengths; plunge/azimuth = orientation of principal axis; K = ellipsoid shape parameter; $\bar{\varepsilon}_s$ = ellipsoid strength parameter

Layer	X (plunge/azimuth)	Y (plunge/azimuth)	Z (plunge/azimuth)	K	$\bar{\varepsilon}_s$
1	1.251 (1.37/191.45)	1.169 (8.12/101.25)	0.684 (81.76/290.93)	0.127	0.468
2	1.158 (6.99/37.07)	1.121 (10.50/128.37)	0.770 (77.35/273.98)	0.085	0.320
3	1.131 (8.59/51.25)	1.092 (8.66/142.57)	0.810 (77.76/277.12)	0.120	0.260
4	1.118 (4.42/28.15)	1.078 (13.57/119.21)	0.830 (75.70/280.48)	0.137	0.230
5	1.113 (11.48/71.62)	1.088 (6.67/162.98)	0.826 (76.68/282.55)	0.084	0.234
6	1.134 (8.33/49.99)	1.114 (8.76/141.28)	0.792 (77.87/277.06)	0.053	0.286
7	1.250 (1.08/192.26)	1.179 (4.00/102.18)	0.678 (85.86/297.34)	0.105	0.477

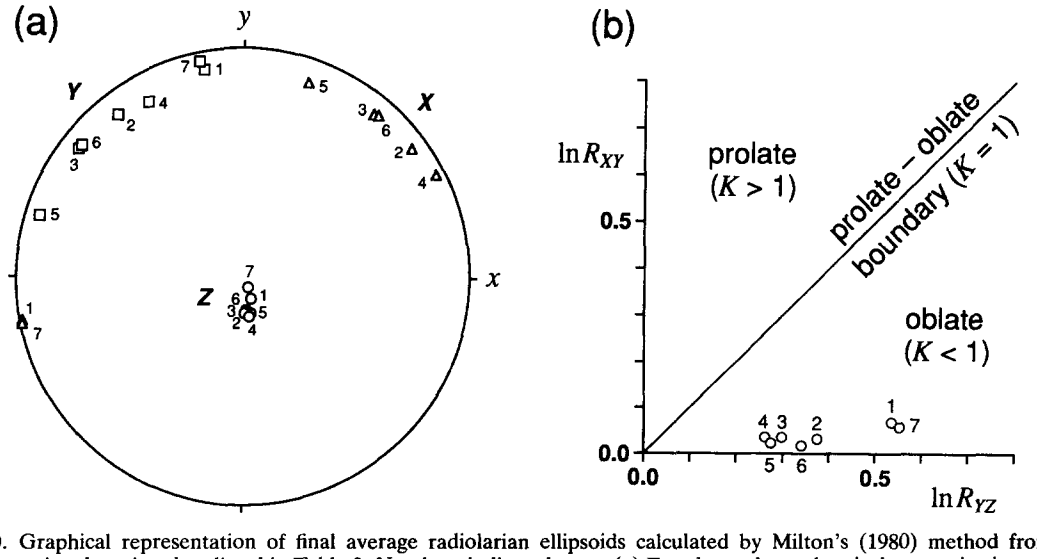

Fig. 10. Graphical representation of final average radiolarian ellipsoids calculated by Milton's (1980) method from two-dimensional section data listed in Table 2. Numbers indicate layers. (a) Equal-area lower-hemisphere projections of three principal ellipsoid axes. Symbols: triangle = X; square = Y; circle = Z. (b) Logarithmic Flinn plot.

Table 5. Corrected final average radiolarian ellipsoids and initial average radiolarian ellipsoids calculated by Wheeler's (1986a) method. ν = constraint parameter; X, Y, Z = principal axial lengths; plunge/aximuth = orientation of principal axis; K = ellipsoid shape parameter; $\bar{\varepsilon}_s$ = ellipsoid strength parameter

		Corrected final radiolarian ellipsoid					Initial radiolarian ellipsoid			
Layer	Constraint ν	X (plunge/azimuth)	Y (plunge/azimuth)	Z (plunge/azimuth)	K	$\bar{\varepsilon}_s$	$X = Y$	Z (plunge/azimuth)	K	$\bar{\varepsilon}_s$
1	−0.048	1.249 (0.21/8.48)	1.169 (7.99/98.51)	0.684 (82.01/276.95)	0.123	0.467	1.053	0.901 (83.97/96.69)	0.000	0.127
2	−0.010	1.157 (7.51/36.56)	1.122 (10.09/127.90)	0.770 (77.38/270.51)	0.082	0.320	1.037	0.929 (84.01/87.78)	0.000	0.090
3	−0.015	1.129 (9.73/52.03)	1.093 (7.12/143.26)	0.810 (77.91/268.89)	0.109	0.259	1.037	0.929 (85.35/85.57)	0.000	0.090
4	−0.030	1.113 (6.65/24.62)	1.082 (12.05/116.05)	0.831 (76.19/266.32)	0.107	0.228	1.038	0.928 (85.68/83.29)	0.000	0.092
5	−0.027	1.112 (12.55/77.76)	1.087 (1.34/168.06)	0.827 (77.38/264.08)	0.084	0.233	1.024	0.954 (85.70/83.52)	0.000	0.058
6	−0.014	1.133 (9.55/51.11)	1.114 (7.16/142.32)	0.792 (78.02/268.63)	0.048	0.286	1.016	0.970 (85.06/87.06)	0.000	0.038
7	−0.023	1.249 (0.25/10.41)	1.180 (3.86/100.42)	0.679 (86.13/276.71)	0.103	0.477	1.069	0.874 (86.79/96.19)	0.000	0.164

Table 6. Radiolarian and matrix cleavage strain ellipsoids. Radiolarian strain ellipsoids are calculated by Wheeler's (1986a) method, while matrix strain ellipsoids are calculated according to Freeman (1987). X, Y, Z = principal axial lengths; plunge/azimuth = orientation of cleavage or principal axis; K = ellipsoid shape parameter; $\bar{\varepsilon}_s$ = strain magnitude parameter

		Radiolarian strain ellipsoid					Matrix strain ellipsoid				
Layer	Cleavage plunge/azimuth	X (plunge/azimuth)	Y (plunge/azimuth)	Z (plunge/azimuth)	K	$\bar{\varepsilon}_s$	X	Y	Z	K	$\bar{\varepsilon}_s$
1	77.08/277.01	1.186 (0.41/8.81)	1.123 (12.91/98.90)	0.750 (77.08/277.01)	0.134	0.354	1.395	1.264	0.567	0.122	0.698
2	71.29/271.20	1.123 (14.17/49.41)	1.090 (11.96/142.48)	0.817 (71.29/271.20)	0.105	0.248	1.223	1.163	0.703	0.099	0.433
3	70.59/270.16	1.099 (17.03/60.51)	1.057 (9.04/153.31)	0.861 (70.59/270.16)	0.187	0.186	1.132	1.077	0.820	0.183	0.245
4	66.14/267.62	1.079 (16.83/40.76)	1.053 (16.41/135.87)	0.881 (66.14/267.62)	0.135	0.157	1.079	1.053	0.881	0.135	0.157
5	72.73/264.22	1.094 (17.21/79.19)	1.062 (1.42/169.63)	0.861 (72.73/264.22)	0.145	0.185	1.137	1.090	0.807	0.141	0.264
6	75.73/268.80	1.119 (12.27/57.57)	1.099 (7.17/149.14)	0.813 (75.73/268.80)	0.061	0.254	1.206	1.172	0.707	0.058	0.425
7	82.46/276.88	1.168 (0.51/10.70)	1.108 (7.52/100.77)	0.773 (82.46/276.88)	0.145	0.318	1.318	1.207	0.629	0.134	0.572

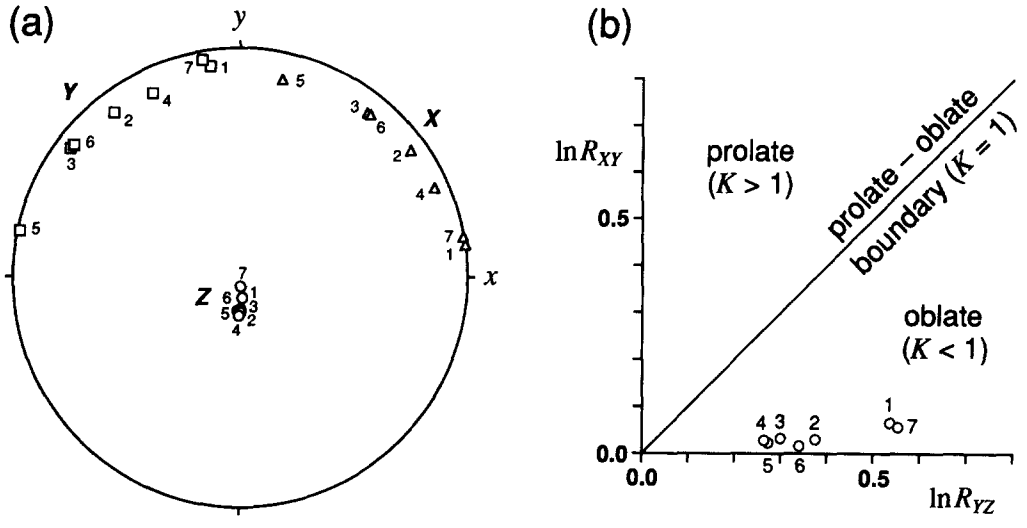

Fig. 11. Graphical representation of final average radiolarian ellipsoids corrected so as to satisfy the constraint ($\nu = 0$) of Wheeler's (1986a) method. Numbers indicate layers. (a) Equal-area lower-hemisphere projections of three principal ellipsoid axes. Symbols: triangle = X; square = Y; circle = Z. (b) Logarithmic Flinn plot.

parallel simple shear. A quartz vein presumed to be initially perpendicular to bedding was used here to estimate layer-parallel shear strains, and hence the effective viscosity ratios in chert–mudstone layers. The results indicate that layer viscosity gradually decreases away from the chert layer with an abrupt change between chert and adjacent mudstone layers (Fig. 7c). But according to this method, the chert/mudstone viscosity ratio never exceeds 6 even in the least competent mudstone layer (Table 3). Folded quartz veins in the chert layer (e.g. Fig. 2a) indicate that vein quartz is much more viscous than the chert, and so the effective viscosity ratios obtained in this study are consistent with those reported elsewhere.

The exact coincidence in the chert layer of both strain ratios calculated from radiolarians and layer-parallel shear strain (Fig. 9) confirms that the viscosity contrast between radiolarians and their chert matrix was negligible during cleavage development. Provided that the viscosity of the radiolarians is constant throughout the layers, the radiolaria/matrix viscosity ratios can therefore be considered equivalent to the chert/mudstone viscosity ratios and can be estimated through layers.

Cleavage refraction

With decreasing competence from the chert layer to mudstone layers, cleavage continuously refracts toward bedding and increases in intensity (Figs. 5 and 6a). Cleavage refraction is also accompanied by a slight but systematic change in cleavage–bedding intersection direction. It could be argued that this variation falls within a statistical error range, and that cleavage–bedding intersections are essentially parallel throughout the layers. But the variation of cleavage orientations on the $x'z'$ section (Figs. 5h–n) seems rather systematic, so the resulting variation of cleavage–bedding intersections is considered not to be an artifact of statistical variations.

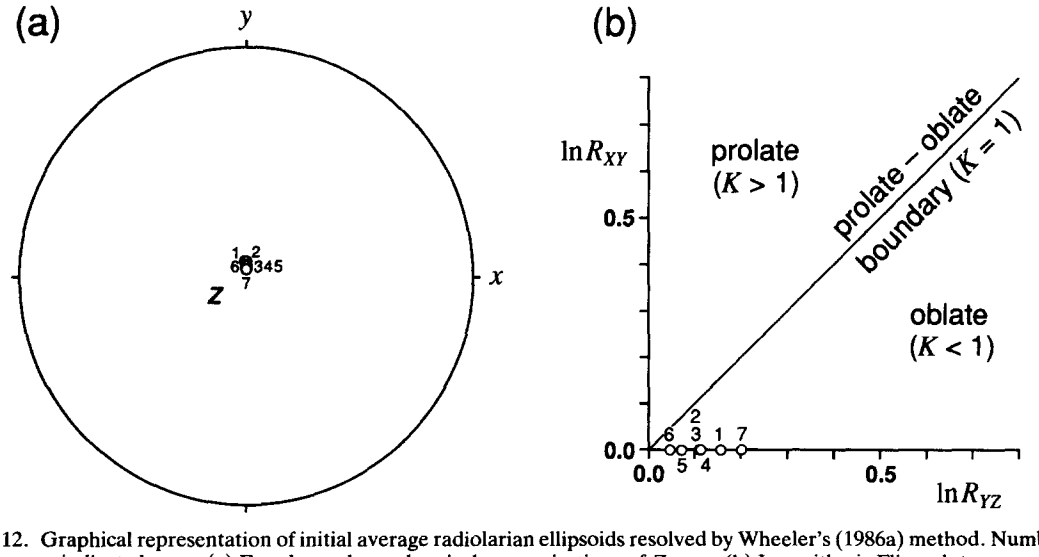

Fig. 12. Graphical representation of initial average radiolarian ellipsoids resolved by Wheeler's (1986a) method. Numbers indicate layers. (a) Equal-area lower-hemisphere projections of Z axes. (b) Logarithmic Flinn plot.

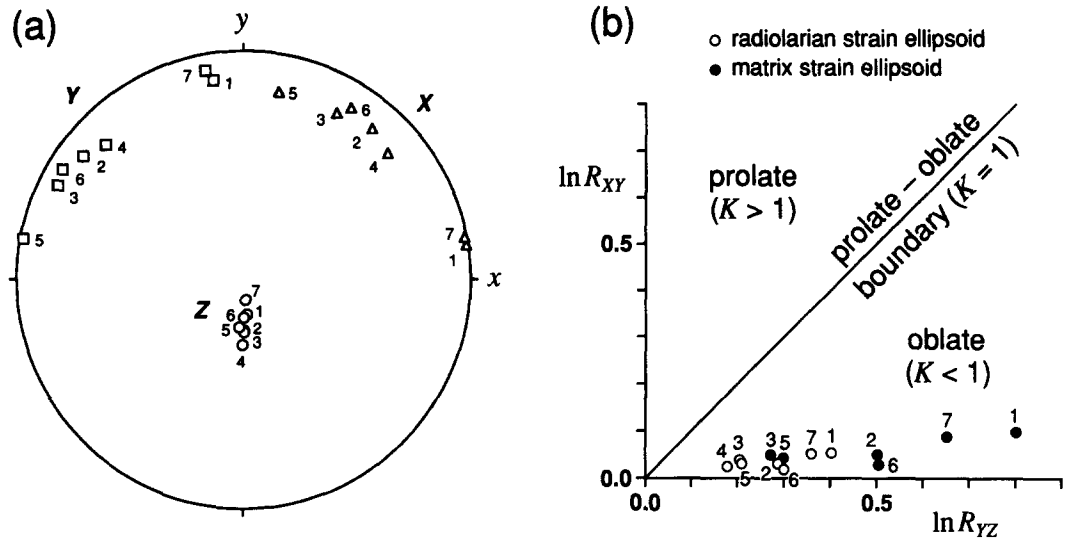

Fig. 13. Graphical representation of cleavage strain ellipsoids for radiolaria and matrix. Numbers indicate layers. Radiolarian strain ellipsoids are calculated by Wheeler's (1986a) method, while matrix strain ellipsoids are calculated according to Freeman (1987). (a) Equal-area lower-hemisphere projections of three principal ellipsoid axes. Symbols: triangle = X; square = Y; circle = Z. (b) Logarithmic Flinn plot. Symbols: open circle = radiolarian strain ellipsoid; filled circle = matrix strain ellipsoid.

Cleavage–bedding intersections rotate anticlockwise as layer competence decreases (Fig. 6b). Finite XY planes subparallel to cleavage should therefore refract such that their intersections with bedding do not remain parallel but rotate anticlockwise with decreasing layer competence. This is consistent with Treagus's (1988) example, and implies a refraction of all three principal axes of finite strain ellipsoid through the layers, hence a three-dimensional strain refraction. Although intersections of XY planes with layering rotate clockwise with decreasing layer competence in Fig. 5 of Treagus (1988), the sense of rotation in her model depends on the direction of layer-parallel shear with respect to layer-parallel–orthogonal strain directions.

The difference in orientation on the $y'z'$ section between the cleavage and the reference vein supposedly initially perpendicular to bedding (Fig. 7a) is too large even in least competent layers to consider this cleavage as initially perpendicular to bedding and afterwards refracted by subsequent strain. This, the second cleavage refraction model of Treagus (1988), where cleavage initiates perpendicular to bedding and subsequently refracts as material planes, is therefore unrealistic for the cleavage here. But this does not necessarily justify her first cleavage refraction model where cleavage refraction exactly represents the refraction of finite XY plane, because cleavage is *a priori* assumed to be parallel to the finite XY plane of cleavage strain in this study.

Strain variation and refraction

Two- and three-dimensional cleavage strains recorded by radiolarians are resolved from their final shapes by Wheeler's (1986a) method using axial ratios and orientations of radiolarians from three sets of sections. Cleavage strains in matrix are then determined from radiolarian strains using radiolaria/matrix viscosity ratios obtained from layer-parallel shear strains and applying Eshelby's equations. The results thus quantify strain refraction across competence contrasts in naturally deformed chert–mudstone layers.

As layer competence decreases, estimated layer-parallel shear strain gradually increases (Fig. 7b), and radiolarian and matrix cleavage strain ellipses gradually increase in axial ratio and refract their long axes parallel to cleavage toward bedding (Fig. 9), which is consistent with the two-dimensional strain refraction theory (Treagus 1983, 1988).

As expected from cleavage refraction, all three principal axes of radiolarian and matrix cleavage strain ellipsoids refract from layer to layer as predicted by Treagus (1983, 1988), indicating a three-dimensional strain refraction. One may argue against this three-dimensional strain refraction maintaining that cleavage–bedding intersections remain subparallel in all layers (Fig. 6b), and therefore that the system must be essentially two-dimensional oblique as expected from Fig. 3(c). But it is never assumed in this study that cleavage directions on the $x'z'$ section are parallel to the principal cleavage strain axis, in which case the system would become essentially two-dimensional oblique. In addition, cleavage–bedding intersections are considered to vary systematically through the layers as discussed earlier, suggesting a three-dimensional strain refraction.

Refractions of X and Y axes through the layers are rather systematic and therefore considered not to be totally an artifact of statistics (Fig. 13a). But their refractions are apparently so significant that a changeover of these axes nearly occurs. Such strong variations of these two axes according to competence contrasts are probably due to cleavage strain ellipsoids close to uniaxial oblate (Fig. 13b), because such ellipsoids with axial lengths $X \approx Y$ have X and Y axes very sensitive to variation in axial length.

Strain magnitude gradually increases away from the chert layer (Table 6). No systematic change in ellipsoid shape occurs associated with strain refraction (Fig. 13b and Table 6), but all are close to uniaxial oblate. This is in contrast to examples considered by Treagus (1983, 1988) where significant variations in strain ellipsoid shape were derived according to competence contrasts. However, the strains in these examples were close to plane strain. Uniaxially oblate strains as in this study may result in no detectable change in strain ellipsoid shape according to competence contrasts.

The radiolarian strain ellipsoids are only slightly more prolate than the corresponding matrix strain ellipsoids (Fig. 13b). Radiolarian strain ellipsoids with very low K values as well as with relatively low viscosity contrasts with matrix may result in such a small difference in strain ellipsoid shape between radiolarians and matrix (cf. appendix 1 in Freeman 1987).

Validities of assumptions and limitations of analyses

The results of strain refraction obtained in this study are internally consistent as indicated below. Cleavage strain systematically refracts through layers. Initial average radiolarian ellipses and ellipsoids in different layers are found to have constant orientations indicating initial bedding (Figs. 8 and 12a). Two-dimensional cleavage strain ratios in matrix calculated from radiolarians reasonably coincide with those calculated from layer-parallel shear strains (Fig. 9). But these internally consistent results do not necessarily imply the validities of assumptions made in this study. The results are reliable if these assumptions are valid or reasonable, but their reliabilities remain uncertain unless the validities of assumptions are assessed.

Basic assumptions made in this study can be summarized as follows. (1) Initial bedding-normal compaction produced quartz veins perpendicular to bedding and a pre-cleavage bedding-symmetric fabric of radiolarians. (2) Average cleavage plane determined is parallel to the finite XY plane of cleavage strain. (3) The chert–mudstone layers were Newtonian viscous during cleavage development. (4) There was no radiolaria/matrix competence contrast in the chert layer during cleavage development, and the viscosity of radiolaria was constant throughout the layers. (5) In radiolarian strain analyses, the cleavage deformation is assumed to be homogeneous such that radiolarians deformed passively as their matrix. (6) In matrix strain calculations, the deformation is assumed to be pure shear in two dimensions, and to be coaxial with constant volume in three dimensions. All other assumptions made can be derived from the above basic assumptions along with observations of the sample. As already discussed earlier, assumptions (1)–(4) are considered to be reasonable, but assumption (5) is reasonable only in the chert layer and incompatible with assumption (6).

Area change and volume reduction are expected to accompany pressure solution during cleavage development (e.g. Wright & Platt 1982, Beutner & Charles 1985). In addition, Treagus's (1988) strain refraction theory indicates that layer-parallel simple shear dominates in incompetent layers, and therefore suggests that the non-coaxial strain component increases as layer competence decreases. Assumption (6) seems therefore unreasonable.

Table 7. Results of unstraining procedures. Unstraining (1) shows axial ratio (R_i) and long-axis orientation (θ) after unstraining of final average radiolarian ellipse by R_s using Bilby & Kolbuszewski's (1977) equations. Unstraining (2) shows strain ratio (R_s), axial ratio (R_i) and long-axis orientation (θ) obtained by unstraining of final average radiolarian ellipse using Bilby & Kolbuszewski's (1977) equations until θ becomes parallel to unstrained bedding

	Unstraining (1)			Unstraining (2)		
Layer	R_s	R_i	θ	R_s	R_i	θ
1	3.66	1.18	−10.7	5.94	1.14	−40.7
2	2.40	1.14	−8.6	2.92	1.11	−26.0
3	1.53	1.13	−4.9	1.59	1.11	−9.9
4	1.21	1.12	−4.4	1.21	1.12	−4.4
5	1.66	1.08	−5.1	1.72	1.07	−10.8
6	2.29	1.04	−5.9	2.41	1.04	−17.2
7	2.77	1.23	−6.0	3.90	1.13	−19.6

As mentioned earlier, competence contrasts between radiolarians and matrix would result in their differential body rotations, the effect of which is ignored by assumption (5). This effect in two dimensions is considered here. For each $y'z'$ domain, the matrix is unstrained with final average radiolarian ellipse (R_f/ϕ) using Bilby & Kolbuszewski's (1977) equations by the amount of matrix strain ratio (R_s) derived from the radiolarians. Their equations are rewritten by Lisle *et al.* (1983) in terms of commonly used variables:

$$G(R_f)\sin 2\phi = G(R_i)\sin 2\theta$$

$$\ln R_s = 2\int_{R_i}^{R_f} \frac{J(R)G(R)}{2R(R+1)^2\sqrt{G^2(R) - G^2(R_i)\sin^2 2\theta}}\,dR,$$

where R_i and θ are the axial ratio and long-axis orientation of the radiolarian ellipse after unstraining, and:

$$J(R) = R^2 + 2rR + 1$$

$$G(R) = \frac{R^2 - 1}{R}\left[\frac{rR^2 + 2R + r}{(R+1)^2}\right]^r,$$

where r is radiolaria/matrix viscosity ratio. Comparison of the results (unstraining (1) in Table 7) with initial average radiolarian ellipses obtained by Wheeler's (1986a) method (R_i/θ in Table 3) indicates that in spite of very small differences in axial ratio the difference in long-axis orientation increases toward less competent layers. This illustrates an increasing component of rigid-body rotation accompanying deformation of radiolarians with increasing competence contrast.

If assumption (5) of bulk homogeneous deformation is dropped, behavior of individual radiolarians as a whole would not be represented by that of an average radiolarian ellipse. Two-dimensional matrix strains can be determined by an unstraining procedure combining the methods of Dunnet & Siddans (1971) and Lisle *et al.* (1983), but no method is available at present for three-

dimensional matrix strains. Possible solutions for two-dimensional matrix strains would be obtained by examining the symmetry of unstrained individual R_f/ϕ data with respect to unstrained bedding at each incremental reciprocal strain, when the symmetry is maximized. Final average radiolarian ellipses are tentatively unstrained here using the above equations until their long axes become parallel to unstrained bedding which is obtained by equation (D.13) of Ramsay & Huber (1983):

$$\tan \theta_b = R_s \tan \phi_b,$$

where ϕ_b and θ_b are bedding directions before and after unstraining, respectively. The results (unstraining (2) in Table 7) indicate that both strain ratios and long-axis orientations of initial radiolarian ellipses deviate significantly in less competent layers from those ($R_s^M(1)$ and θ in Table 3) obtained by combined methods of Bilby *et al.* (1975) and Wheeler (1986a). This procedure, however, yields internally inconsistent results with initial bedding directions varying significantly through layers. Although the unstraining procedure of individual R_f/ϕ data requires a huge amount and time of calculations, this is definitely the next step to be done.

CONCLUSIONS

A sample of chert–mudstone layers used in this study provides a rare example of quantitative analyses of competence contrasts in naturally deformed rocks, because it contains deformed quartz veins some of which were possibly formed subperpendicular to bedding before cleavage development, and also abundant radiolarians used as strain markers whose viscosity during deformation is approximated by that of chert. Under several assumptions these enabled tentative quantitative analyses leading to the following conclusions which seem to be consistent with Treagus's (1983, 1988) strain refraction theory.

(1) Effective layer viscosity ratios were estimated from layer-parallel shear strains using a vein supposed to be initially perpendicular to bedding. Chert/mudstone layer viscosity ratios so obtained (2.6–5.7) were used as radiolaria/matrix viscosity ratios in different layers.

(2) With decreasing layer competence, cleavage refracts towards bedding and increases in intensity, while cleavage–bedding intersections do not remain parallel but rotate anticlockwise. Finite XY planes subparallel to cleavage should refract in this way, and all three principal axes of finite strain ellipsoids should refract through layers of different competences.

(3) As expected from cleavage refraction, all three principal axes of radiolarian and matrix strain ellipsoids estimated in this study refract from layer to layer. Strain magnitude systematically varies according to layer competence. However, no systematic change in ellipsoid shape associated with strain refraction is recognized.

(4) Strain ratios calculated from radiolarians taking account of competence contrast with their matrix reasonably coincide with strain ratios calculated from layer-parallel shear strains. Initial average radiolarian ellipses and ellipsoids obtained have constant orientations with respect to initial bedding through layers. These, along with systematic strain refraction, make the results internally consistent.

(5) The above results are reliable if several assumptions made are valid or reasonable. Some assumptions seem reasonable. But others are unreasonable and thus bring uncertainties in the results obtained.

Acknowledgements—I thank Susan Treagus whose previous works motivated me to this study. Her detailed and thorough review significantly improved the manuscript. An anonymous reviewer is also thanked for suggesting a proper use of Wheeler's method. This study was supported by Grant 03740400 from the Ministry of Education, Science and Culture of Japan.

REFERENCES

Beutner, E. C. & Charles, E. G. 1985. Large volume loss during cleavage formation, Hamburg sequence, Pennsylvania. *Geology* **13**, 803–805.

Bilby, B. A., Eshelby, J. D. & Kundu, A. K. 1975. The change of shape of a viscous ellipsoidal region embedded in a slowly deforming matrix having a different viscosity. *Tectonophysics* **28**, 265–274.

Bilby, B. A. & Kolbuszewski, M. L. 1977. The finite deformation of an inhomogeneity in two-dimensional slow viscous incompressible flow. *Proc. R. Soc. Lond.* **A355**, 335–353.

Biot, M. A. 1965a. Theory of viscous buckling and gravity instability of multilayers with large deformation. *Bull. geol. Soc. Am.* **76**, 371–378.

Biot, M. A. 1965b. *Mechanics of Incremental Deformations*. John Wiley & Sons, New York.

Cobbold, P. R. 1983. Kinematic and mechanical discontinuity at a coherent interface. *J. Struct. Geol.* **5**, 341–349.

De Paor, D. G. 1990. Determination of the strain ellipsoid from sectional data. *J. Struct. Geol.* **12**, 131–137.

Dunnet, D. & Siddans, A. W. B. 1971. Non-random sedimentary fabrics and their modifications by strain. *Tectonophysics* **12**, 307–325.

Eshelby, J. D. 1957. The determination of the elastic field of an ellipsoidal inclusion, and related problems. *Proc. R. Soc. Lond.* **A241**, 376–396.

Freeman, B. 1987. The behaviour of deformable ellipsoidal particles in three-dimensional slow flows: implications for geological strain analysis. *Tectonophysics* **132**, 297–309.

Freeman, B. & Lisle, R. J. 1987. The relationship between tectonic strain and the three-dimensional shape fabrics of pebbles in deformed conglomerates. *J. geol. Soc. Lond.* **144**, 635–639.

Gay, N. C. 1968a. Pure shear and simple shear deformation of inhomogeneous viscous fluids—I. Theory. *Tectonophysics* **5**, 211–234.

Gay, N. C. 1968b. Pure shear and simple shear deformation of inhomogeneous viscous fluids—II. The determination of the total finite strain in a rock from objects such as deformed pebbles. *Tectonophysics* **5**, 292–302.

Gay, N. C. 1969. The analysis of strain in the Barberton Mountain Land, Eastern Transvaal, using deformed pebbles. *J. Geol.* **77**, 377–396.

Gay, N. C. & Jaeger, J. C. 1975. Cataclastic deformation of geological materials in matrices of differing composition: I. Pebbles and conglomerates. *Tectonophysics* **27**, 303–322.

Gay, N. C. & Fripp, R. E. P. 1976. The control of ductility on the deformation of pebbles and conglomerates. *Phil. Trans. R. Soc. Lond.* **A283**, 109–128.

Harker, A. 1886. On slaty cleavage and allied rock structures, with special reference to the mechanical theories of their origin. *Rep. Br. Ass. Adv. Sci.* (1885), 813–852.

Hobbs, B. E., Means, W. D. & Williams, P. F. 1976. *An Outline of Structural Geology*. John Wiley & Sons, New York.

Kanagawa, K. 1990. Automated two-dimensional strain analysis from deformed elliptical markers using an image analysis system. *J. Struct. Geol.* **12**, 139–143.

Kanagawa, K. 1991. Change in dominant mechanisms for phyllosilicate preferred orientation during cleavage development in the Kitakami slates of NE Japan. *J. Struct. Geol.* **13**, 927–943.
Knipe, R. J. 1989. Deformation mechanisms—recognition from natural tectonites. *J. Struct. Geol.* **11**, 127–946.
Lisle, R. J. 1985. *Geological Strain Analysis: A Manual for the R_f/ϕ Technique*. Pergamon Press, Oxford.
Lisle, R. J. & Savage, J. F. 1982. Factors influencing rock competence: Data from a Swedish deformed conglomerate. *Geol. Föl. Stockh. Förh.* **104**, 219–224.
Lisle, R. J., Rondeel, H. E., Doorn, D., Brugge, J. & van de Gaag, P. 1983. Estimation of viscosity contrast and finite strain from deformed elliptical inclusions. *J. Struct. Geol.* **5**, 603–609.
Means, W. D. 1990. Kinematics, stress, deformation and material behavior. *J. Struct. Geol.* **12**, 953–971.
Milton, N. J. 1980. Determination of the strain ellipsoid from measurements on any three sections. *Tectonophysics* **64**, T19–T27.
Nadai, A. 1963. *Theory of Flow and Fracture of Solids, Volume* II. McGraw-Hill, New York.
Owens, W. H. 1984. The calculation of a best-fit ellipsoid from elliptical sections on arbitrarily oriented planes. *J. Struct. Geol.* **6**, 571–578.
Peach, C. J. & Lisle, R. J. 1979. A FORTRAN IV program for the analysis of tectonic strain using deformed elliptical markers. *Comput. & Geosci.* **5**, 325–334.
Price, N. J. & Cosgrove, J. W. 1990. *Analysis of Geological Structures*. Cambridge University Press, Cambridge.
Ramsay, J. G. 1967. *Folding and Fracturing of Rocks*. McGraw-Hill, New York.
Ramsay, J. G. 1982. Rock ductility and its influence on the development of tectonic structures in mountain belts. In: *Mountain Building Processes* (edited by Hsü, K. J.). Academic Press, London, 117–127.
Ramsay, J. G. & Huber, M. I. 1983. *The Techniques of Modern Structural Geology, Volume* 1: *Strain Analysis*. Academic Press, London.
Ramsay, J. G. & Huber, M. I. 1987. *The Techniques of Modern Structural Geology, Volume* 2: *Folds and Fractures*. Academic Press, London.
Rutter, E. H. 1976. The kinetics of rock deformation by pressure solution. *Phil. Trans. R. Soc. Lond.* **A283**, 203–219.
Rutter, E. H. 1983. Pressure solution in nature, theory and experiment. *J. geol. Soc. Lond.* **140**, 725–740.
Sherwin, J. & Chapple, W. M. 1968. Wavelengths of single layer folds: a comparison between theory and observation. *Am. J. Sci.* **266**, 167–179.
Shimamoto, T. & Hara, I. 1976. Geometry and strain distribution of single-layer folds. *Tectonophysics* **30**, 1–34.
Shimamoto, R. & Ikeda, Y. 1976. A simple algebraic method for strain estimation from deformed ellipsoidal objects—1. Basic theory. *Tectonophysics* **36**, 315–337.
Sorby, H. C. 1853. On the origin of slaty cleavage. *Edinb. New Philos. J.* **55**, 137–148.
Spiers, C. J. & Schutjens, P. M. T. M. 1990. Densification of crystalline aggregates by fluid-phase diffusional creep. In: *Deformation Processes in Minerals, Ceramics and Rocks* (edited by Barber, D. J. & Meredith, P.G.). Unwin Hyman, London, 334–353.
Tan, B. K. 1974. Deformation of particles developed around rigid and deformable nuclei. *Tectonophysics* **24**, 243–257.
Treagus, S. H. 1973. Buckling stability of a viscous single-layer system, oblique to the principal compression. *Tectonophysics* **19**, 271–289.
Treagus, S. H. 1981. A theory of stress and strain variations in viscous layers, and its geological implications. *Tectonophysics* **72**, 75–103.
Treagus, S. H. 1983. A theory of finite strain variation through contrasting layers, and its bearing on cleavage refraction. *J. Struct. Geol.* **5**, 351–368.
Treagus, S. H. 1988. Strain refraction in layered systems. *J. Struct. Geol.* **10**, 517–527.
Treagus, S. H. & Sokoutis, D. 1992. Laboratory modelling of strain variation across rheological boundaries. *J. Struct. Geol.* **14**, 405–424.
Weijermars, R. 1992. Progressive deformation in anisotropic rocks. *J. Struct. Geol.* **14**, 723–742.
Wheeler, J. 1984. A new plot to display the strain of elliptical markers. *J. Struct. Geol.* **6**, 417–423.
Wheeler, J. 1986a. Strain analysis in rocks with pretectonic fabrics. *J. Struct. Geol.* **8**, 887–896.
Wheeler, J. 1986b. Average properties of ellipsoidal fabrics: implications for two- and three-dimensional methods of strain analysis. *Tectonophysics* **126**, 259–270.
Wright, T. O. & Platt, L. B. 1982. Pressure dissolution and cleavage in the Martinsburg shale. *Am. J. Sci.* **182**, 122–135.

APPENDIX 1
STRAIN ANALYSIS OF ELLIPTICAL/ ELLIPSOIDAL MARKERS WITH AN INITIAL BEDDING-SYMMETRIC FABRIC: WHEELER'S (1986a) METHOD

Notation

i, f	subscripts denoting initial and final
T	superscript denoting transposed vector or tensor
x	position (column) vector
b	unit vector normal to bedding
c	unit vector normal to cleavage
l	unit vector parallel to lineation (cleavage trace in two dimensions)
m	unit vector parallel to cleavage–bedding intersection
E	unit tensor
F	symmetric second-order tensor
G	Shimamoto & Ikeda's (1976) ellipse shape tensor
H	Wheeler's (1984) ellipse shape tensor
M	Shimamoto & Ikeda's (1976) shape tensor of average marker ellipse
N	Wheeler's (1984) shape tensor of average marker ellipse/ellipsoid
a_1, a_2, a_3	eigenvalues of **N** ($a_1 \geq a_2 \geq a_3$, $a_1a_2a_3 = 1$)
P	deformation (position gradient) tensor
L	Finger's tensor ($\mathbf{L} = \mathbf{PP}^T$)
Δ	dilatation
D	non-dilatational deformation tensor
$\mathbf{N}_s$	Wheeler's (1984) shape tensor for strain ellipse/ ellipsoid
$\lambda_1, \lambda_2, \lambda_3$	eigenvalues of $\mathbf{N}_s$ ($\lambda_1 \geq \lambda_2 \geq \lambda_3$, $\lambda_1\lambda_2\lambda_3 = 1$)
u	vector defined by $\mathbf{N}_f\mathbf{b}_f$
u′	unit vector parallel to **u**
v	vector defined by $\mathbf{N}_f\mathbf{c}$
v′	unit vector parallel to **v**
ν	constraint parameter in three-dimensional analysis

Average marker ellipse

Any ellipse can be described by the following equation:

$$\mathbf{x}^T\mathbf{F}\mathbf{x} = 1, \tag{A1}$$

where **F** is a symmetric second-order tensor. Shimamoto & Ikeda's (1976) ellipse shape tensor is a tensor of unit determinant defined as:

$$\mathbf{G} = \frac{\mathbf{F}}{\sqrt{|\mathbf{F}|}}, \tag{A2}$$

where $|\mathbf{F}|$ is the determinant of **F**. Wheeler's (1984) ellipse shape tensor is also a tensor of unit determinant defined as:

$$\mathbf{H} = \frac{\mathbf{F}^{-1}}{\sqrt{|\mathbf{F}^{-1}|}}, \tag{A3}$$

where

$$\mathbf{H} = \mathbf{G}^{-1} \tag{A4}$$

because

$$\mathbf{GH} = \frac{\mathbf{FF}^{-1}}{\sqrt{|\mathbf{F}||\mathbf{F}^{-1}|}} = \mathbf{E} \qquad \left(\because |\mathbf{F}^{-1}| = \frac{1}{|\mathbf{F}|}\right).$$

Both shape tensors represent the same ellipse scaled to area π from the ellipse (A1). Both tensors have their eigenvectors parallel to the ellipse axes. The eigenvalues of Shimamoto & Ikeda's (1976) shape tensor give reciprocal squared axial lengths of the ellipse, whereas those of Wheeler's (1984) shape tensor give squared axial lengths. For an ellipse with axial ratio R and long-axis orientation ϕ from the x axis, **G** and **H** are given by the following equations:

$$\mathbf{G} = \begin{bmatrix} R\sin^2\phi + \frac{1}{R}\cos^2\phi & \left(\frac{1}{R} - R\right)\sin\phi\cos\phi \\ \left(\frac{1}{R} - R\right)\sin\phi\cos\phi & \frac{1}{R}\sin^2\phi + R\cos^2\phi \end{bmatrix} \quad \text{(A5)}$$

$$\mathbf{H} = \begin{bmatrix} \frac{1}{R}\sin^2\phi + R\cos^2\phi & \left(R - \frac{1}{R}\right)\sin\phi\cos\phi \\ \left(R - \frac{1}{R}\right)\sin\phi\cos\phi & R\sin^2\phi + \frac{1}{R}\cos^2\phi \end{bmatrix} \quad \text{(A6)}$$

For a suite of marker ellipses, shape tensors for individual marker ellipses can be averaged by adding them and dividing by the number of ellipses (Wheeler 1984, 1986b). Two types of averaged shape tensor are written here as $\bar{\mathbf{G}}$ and $\bar{\mathbf{H}}$. The average marker ellipse is one with area π represented by either of the following shape tensors:

$$\mathbf{M} = \frac{\bar{\mathbf{G}}}{\sqrt{|\bar{\mathbf{G}}|}} \quad \text{(A7)}$$

$$\mathbf{N} = \frac{\bar{\mathbf{H}}}{\sqrt{|\bar{\mathbf{H}}|}}. \quad \text{(A8)}$$

For two dimensions it is proved by Wheeler (1986b) that:

$$\mathbf{N} = \mathbf{M}^{-1}. \quad \text{(A9)}$$

M and **N** equally represent the average marker ellipse: both have eigenvectors parallel to the axes of average marker ellipse; and **M** has eigenvalues of recriprocal squared axial lengths, whereas **N** has those of squared axial lengths. If marker ellipses were initially randomly oriented and are deformed homogeneously, the final average marker ellipse would be identical to the strain ellipse scaled to area π (Shimamoto & Ikeda 1976, Wheeler 1984).

Non-dilatational part of deformation

Any deformation can be described by a position gradient tensor **P**. The strain ellipse/ellipsoid can then be described by the following equation:

$$\mathbf{x}^{\mathrm{T}}\mathbf{L}^{-1}\mathbf{x} = 1, \quad \text{(A10)}$$

where **L** is the Finger's tensor such that:

$$\mathbf{L} = \mathbf{P}\mathbf{P}^{\mathrm{T}}. \quad \text{(A11)}$$

Wheeler's (1984) shape tensor for the strain ellipse/ellipsoid is given as follows:

$$\mathbf{N}_{\mathrm{s}} = \frac{\mathbf{L}}{|\mathbf{L}|^{1/n}}, \quad \text{(A12)}$$

where $|\mathbf{L}|$ is equal to square of the dilatational strain, $1 + \Delta$, and n is the dimensionality 2 or 3. $\mathbf{N}_{\mathrm{s}}$ represents the strain ellipse/ellipsoid scaled to area π in two dimensions or volume $4\pi/3$ in three dimensions, and its eigenvalues ($\lambda_1 \geq \lambda_2 \geq \lambda_3$, $\lambda_1\lambda_2\lambda_3 = 1$) are equal to squared axial lengths of the ellipse/ellipsoid. If the deformation conserves area/volume, then $\mathbf{N}_{\mathrm{s}}$ exactly represents the strain ellipse/ellipsoid. Substituting (A11) into (A12) and rearranging:

$$\mathbf{N}_{\mathrm{s}} = \frac{\mathbf{P}}{|\mathbf{P}|^{1/n}}\frac{\mathbf{P}^{\mathrm{T}}}{|\mathbf{P}^{\mathrm{T}}|^{1/n}}. \quad \text{(A13)}$$

Defining the non-dilatational deformation tensor, **D**, by:

$$\mathbf{D} = \frac{\mathbf{P}}{|\mathbf{P}|^{1/n}}. \quad \text{(A14)}$$

(A13) can be rewritten as:

$$\mathbf{N}_{\mathrm{s}} = \mathbf{D}\mathbf{D}^{\mathrm{T}}. \quad \text{(A15)}$$

Thus $\mathbf{N}_{\mathrm{s}}$ represents the non-dilatational part of the deformation. Because we are dealing only with the shapes of ellipses/ellipsoids in this study, (A15) is sufficient to describe their changes during the deformation. If both $\mathbf{N}_{\mathrm{s}}$ and Δ are determined, **L** is then found from (A12) as:

$$\mathbf{L} = (1 + \Delta)^{2/n}\mathbf{N}_{\mathrm{s}}. \quad \text{(A16)}$$

Two-dimensional strain analysis on a section plane

Initial bedding-symmetric condition in two dimensions implies that the long axis of initial average marker ellipse is parallel to the initial bedding trace. The shape tensor for such an ellipse has an eigenvalue a_2 ($=1/a_1$) in the bedding-normal direction, and therefore:

$$\mathbf{N}_{\mathrm{i}}\mathbf{b}_{\mathrm{i}} = a_2\mathbf{b}_{\mathrm{i}}. \quad \text{(A17)}$$

$\mathbf{N}_{\mathrm{f}}$ and $\mathbf{b}_{\mathrm{f}}$ are related to $\mathbf{N}_{\mathrm{i}}$ and $\mathbf{b}_{\mathrm{i}}$ by non-dilatational deformation tensors as follows (Wheeler 1986a):

$$\mathbf{N}_{\mathrm{f}} = \mathbf{D}\mathbf{N}_{\mathrm{i}}\mathbf{D}^{\mathrm{T}} \quad \text{(A18)}$$

$$\mathbf{b}_{\mathrm{f}} = \frac{(\mathbf{D}^{\mathrm{T}})^{-1}\mathbf{b}_{\mathrm{i}}}{|(\mathbf{D}^{\mathrm{T}})^{-1}\mathbf{b}_{\mathrm{i}}|}, \quad \text{(A19)}$$

where $|(\mathbf{D}^{\mathrm{T}})^{-1}\mathbf{b}_{\mathrm{i}}|$ is the norm of $(\mathbf{D}^{\mathrm{T}})^{-1}\mathbf{b}_{\mathrm{i}}$. $\mathbf{N}_{\mathrm{i}}$ and $\mathbf{b}_{\mathrm{i}}$ can then be expressed in terms of $\mathbf{N}_{\mathrm{f}}$ and $\mathbf{b}_{\mathrm{f}}$ as follows:

$$\mathbf{N}_{\mathrm{i}} = \mathbf{D}^{-1}\mathbf{N}_{\mathrm{f}}(\mathbf{D}^{\mathrm{T}})^{-1} \quad \text{(A20)}$$

$$\mathbf{b}_{\mathrm{i}} = \frac{\mathbf{D}^{\mathrm{T}}\mathbf{b}_{\mathrm{f}}}{|\mathbf{D}^{\mathrm{T}}\mathbf{b}_{\mathrm{f}}|}. \quad \text{(A21)}$$

Substituting (A20) and (A21) into (A17), we get:

$$\mathbf{D}^{-1}\mathbf{N}_{\mathrm{f}}\mathbf{b}_{\mathrm{f}} = a_2\mathbf{D}^{\mathrm{T}}\mathbf{b}_{\mathrm{f}}. \quad \text{(A22)}$$

Multiplying both sides of (A22) with a preceding **D**, and using $\mathbf{N}_{\mathrm{s}} = \mathbf{D}\mathbf{D}^{\mathrm{T}}$ and $\mathbf{u} = \mathbf{N}_{\mathrm{f}}\mathbf{b}_{\mathrm{f}}$:

$$\mathbf{u} = a_2\mathbf{N}_{\mathrm{s}}\mathbf{b}_{\mathrm{f}}. \quad \text{(A23)}$$

Wheeler (1986a) describes the geometrical significance of $\mathbf{N}_{\mathrm{f}}\mathbf{b}_{\mathrm{f}}$. Dot-multiplying both sides of (A23) with **l**, and using $\mathbf{l}\cdot(\mathbf{N}_{\mathrm{s}}\mathbf{b}_{\mathrm{f}}) = (\mathbf{N}_{\mathrm{s}}\mathbf{l})\cdot\mathbf{b}_{\mathrm{f}}$ because $\mathbf{N}_{\mathrm{s}}$ is symmetrical:

$$\mathbf{l}\cdot\mathbf{u} = a_2(\mathbf{N}_{\mathrm{s}}\mathbf{l})\cdot\mathbf{b}_{\mathrm{f}}. \quad \text{(A24)}$$

Dot-multiplying both sides of (A23) with **c** similarly yields:

$$\mathbf{c}\cdot\mathbf{u} = a_2(\mathbf{N}_{\mathrm{s}}\mathbf{c})\cdot\mathbf{b}_{\mathrm{f}}. \quad \text{(A25)}$$

Since $\mathbf{N}_{\mathrm{s}}$ has eigenvalues λ_1 and λ_2 ($= 1/\lambda_1$) with eigenvectors **l** and **c**, respectively,

$$\mathbf{N}_{\mathrm{s}}\mathbf{l} = \lambda_1\mathbf{l} \quad \text{(A26)}$$

$$\mathbf{N}_{\mathrm{s}}\mathbf{c} = \frac{1}{\lambda_1}\mathbf{c}. \quad \text{(A27)}$$

Substituting (A26) and (A27) in (A24) and (A25), respectively, we get:

$$\mathbf{l}\cdot\mathbf{u} = \lambda_1 a_2\mathbf{l}\cdot\mathbf{b}_{\mathrm{f}} \quad \text{(A28)}$$

$$\mathbf{c}\cdot\mathbf{u} = \frac{a_2}{\lambda_1}\mathbf{c}\cdot\mathbf{b}_{\mathrm{f}}. \quad \text{(A29)}$$

(A28) and (A29) are two equations with two unknowns, λ_1 and a_2. Solving these equations with respect to λ_1 and a_2 yields:

$$\lambda_1^2 = \frac{(\mathbf{l}\cdot\mathbf{u})(\mathbf{c}\cdot\mathbf{b}_{\mathrm{f}})}{(\mathbf{c}\cdot\mathbf{u})(\mathbf{l}\cdot\mathbf{b}_{\mathrm{f}})} \quad \text{(A30)}$$

$$a_2^2 = \frac{(\mathbf{l}\cdot\mathbf{u})(\mathbf{c}\cdot\mathbf{u})}{(\mathbf{l}\cdot\mathbf{b}_{\mathrm{f}})(\mathbf{c}\cdot\mathbf{b}_{\mathrm{f}})}. \quad \text{(A31)}$$

(A30) and (A31) must satisfy $\lambda_1^2 > 1$ and $a_2^2 < 1$ such that they are geologically realistic. The axial ratio of strain ellipse, R_{s}, is equal to λ_1, because:

$$R_{\mathrm{s}} = \sqrt{\frac{\lambda_1}{\lambda_2}} = \sqrt{\lambda_1^2} = \lambda_1 \quad \left(\because \lambda_2 = \frac{1}{\lambda_1}\right).$$

The strain-ellipse long axis is parallel to **l**, and its orientation ϕ_{s} is given by the cleavage trace direction. $\mathbf{N}_{\mathrm{s}}$ is obtained from R_{s} and ϕ_{s} using the equation similar to (A6):

$$\mathbf{N}_{\mathrm{s}} = \begin{bmatrix} \frac{1}{R}\sin^2\phi_{\mathrm{s}} + R\cos^2\phi_{\mathrm{s}} & \left(R - \frac{1}{R_{\mathrm{s}}}\right)\sin\phi_{\mathrm{s}}\cos\phi_{\mathrm{s}} \\ \left(R_{\mathrm{s}} - \frac{1}{R_{\mathrm{s}}}\right)\sin\phi_{\mathrm{s}}\cos\phi_{\mathrm{s}} & R_{\mathrm{s}}\sin^2\phi_{\mathrm{s}} + \frac{1}{R_{\mathrm{s}}}\cos^2\phi_{\mathrm{s}} \end{bmatrix}. \quad \text{(A32)}$$

The non-dilatational deformation tensor **D** is then found from $\mathbf{N}_s = \mathbf{DD}^T$. Substituting this **D** into (A21) and (A20) gives the initial bedding direction and the initial average marker ellipse, respectively, the latter having the axis of length $\sqrt{a_2}$ perpendicular to the initial bedding.

Three-dimensional strain analysis assuming initial average marker ellipsoid of uniaxially oblate shape

An initial average marker ellipsoid of uniaxially oblate shape will have the axial length of $\sqrt{a_1} = \sqrt{a_2}$ in any direction parallel to the initial bedding, and that of $\sqrt{a_3} = 1/a_1$ in the direction normal to bedding. The shape tensor of such an ellipsoid can be written as follows (Wheeler 1986a):

$$\mathbf{N}_i = a_1\mathbf{E} + \left(\frac{1}{a_1^2} - a_1\right)\mathbf{b}_i\mathbf{b}_i^T. \tag{A33}$$

Substituting (A33) into (A18):

$$\begin{aligned}\mathbf{N}_f &= a_1\mathbf{DED}^T + \left(\frac{1}{a_1^2} - a_1\right)\mathbf{D}(\mathbf{b}_i\mathbf{b}_i^T)\mathbf{D}^T \\ &= a_1\mathbf{N}_s + \left(\frac{1}{a_1^2} - a_1\right)(\mathbf{Db}_i)(\mathbf{Db}_i)^T.\end{aligned} \tag{A34}$$

Multiplying both sides of (A21) with a preceding **D**:

$$\mathbf{Db}_i = \frac{\mathbf{N}_s\mathbf{b}_f}{|\mathbf{D}^T\mathbf{b}_f|}. \tag{A35}$$

The denominator of the right-hand side of (A35) and be rewritten as:

$$|\mathbf{D}^T\mathbf{b}_f| = \sqrt{\mathbf{D}^T\mathbf{b}_f \cdot \mathbf{D}^T\mathbf{b}_f}, \tag{A36}$$

where

$$\mathbf{D}^T\mathbf{b}_f \cdot \mathbf{D}^T\mathbf{b}_f = (\mathbf{D}^T\mathbf{b}_f)^T\mathbf{D}^T\mathbf{b}_f = \mathbf{b}_f^T\mathbf{DD}^T\mathbf{b}_f = \mathbf{b}_f \cdot \mathbf{N}_s\mathbf{b}_f.$$

Therefore:

$$|\mathbf{D}^T\mathbf{b}_f| = \sqrt{\mathbf{b}_f \cdot \mathbf{N}_s\mathbf{b}_f}. \tag{A37}$$

Substituting (A37) into (A35) and applying (A23):

$$\mathbf{Db}_i = \frac{\mathbf{u}}{\sqrt{a_3\mathbf{b}_f \cdot \mathbf{u}}}. \tag{A38}$$

Substituting (A38) into (A34) and using $a_3 = 1/a_1^2$:

$$\mathbf{N}_f = a_1\mathbf{N}_s + \frac{1 - a_1^3}{\mathbf{b}_f \cdot \mathbf{u}}\mathbf{uu}^T. \tag{A39}$$

Dot-multiplying both sides of (A39) with **c** and using $\mathbf{v} = \mathbf{N}_f\mathbf{c}$ yields:

$$\mathbf{v} = a_1\lambda_3\mathbf{c} + (1 - a_1^3)\frac{\mathbf{c} \cdot \mathbf{u}}{\mathbf{b}_f \cdot \mathbf{u}}\mathbf{u}. \tag{A40}$$

The geometrical significance of **v** is described by Wheeler (1986a). (A40) indicates that three vectors **v**, **c** and **u** are coplanar, and provides a constraint parameter as follows:

$$v = \mathbf{c} \cdot (\mathbf{v}' \times \mathbf{u}') = 0. \tag{A41}$$

$\mathbf{N}_f$ must be corrected so as to exactly satisfy this constraint before any other calculations. A correction is suggested by Wheeler (1986a) as follows:

$$\mathbf{K}^{-1} = \mathbf{N}_f^{-1} - (\mathbf{c} \cdot \mathbf{N}_f^{-1}\mathbf{m})(\mathbf{mc} + \mathbf{cm}) \tag{A42}$$

$$\mathbf{N}_f^c = \frac{\mathbf{K}}{|\mathbf{K}|^{1/3}}, \tag{A43}$$

where $\mathbf{N}_f^c$ is the corrected final average marker ellipsoid. Dot-multiplying both sides of (A40) with **c** yields:

$$\mathbf{c} \cdot \mathbf{v} = a_1\lambda_3 + (1 - a_1^3)\frac{(\mathbf{c} \cdot \mathbf{u})^2}{\mathbf{b}_f \cdot \mathbf{u}}. \tag{A44}$$

Dot-multiplying both sides of (A40) with $\mathbf{b}_f$ gives:

$$\mathbf{u} \cdot \mathbf{c} = a_1\lambda_3\mathbf{c} \cdot \mathbf{b}_f + (1 - a_1^3)(\mathbf{c} \cdot \mathbf{u}) \tag{A45}$$

because:

$$\mathbf{b}_f \cdot \mathbf{v} = \mathbf{b}_f \cdot \mathbf{N}_f\mathbf{c} = \mathbf{N}_f\mathbf{b}_f \cdot \mathbf{c} = \mathbf{u} \cdot \mathbf{c}.$$

(A44) and (A45) are two equations with two unknowns, a_1 and λ_3. Solving these equations with respect to a_1 yields:

$$a_1^3 = \frac{(\mathbf{c} \cdot \mathbf{b}_f)(\mathbf{c} \cdot \mathbf{v})(\mathbf{b}_f \cdot \mathbf{u}) - (\mathbf{c} \cdot \mathbf{u})^2}{(\mathbf{c} \cdot \mathbf{u})\{\mathbf{b}_f \cdot \mathbf{u} - (\mathbf{c} \cdot \mathbf{b}_f)(\mathbf{c} \cdot \mathbf{u})\}}. \tag{A46}$$

Using a_1 thus obtained. $\mathbf{N}_s$ can be calculated from (A39) as:

$$\mathbf{N}_s = \frac{1}{a_1}\mathbf{N}_f + \left(a_1^2 - \frac{1}{a_1}\right)\frac{\mathbf{uu}^T}{\mathbf{b}_f \cdot \mathbf{u}}. \tag{A47}$$

The non-dilatational part of the deformation is thus determined. The eigenvectors and eigenvalues of $\mathbf{N}_s$ give the principal axes and squared axial lengths of the strain ellipsoid scaled to volume $4\pi/3$. The non-dilatational deformation tensor **D** is then found from $\mathbf{N}_s = \mathbf{DD}^T$. Substituting this **D** into (A20) gives the initial uniaxial average marker ellipsoid which has axial length of $\sqrt{a_1}$ parallel to the initial bedding.

APPENDIX 2
ESTIMATION OF MATRIX STRAINS FROM COMPETENT ELLIPTICAL/ELLIPSOIDAL INCLUSIONS: APPLICATIONS OF ESHELBY'S (1957) EQUATIONS

Notation

I,M	superscripts denoting inclusion and matrix
a_i	axial length of inclusion
X, Y, Y	axial length of strain ellipsoid ($X \geq Y \geq Z$)
ε_{ij}	natural strain tensor
$\dot{\varepsilon}_{ij}$	strain rate tensor
ω_{ij}	vorticity tensor
S_{ijkl}	tensor relating matrix and inclusion strain rates
Π_{ijkl}	tensor relating matrix and inclusion vorticities
μ	viscosity
r	viscosity ratio ($r = \mu^I/\mu^M$)
R	strain ratio.

Deformation of a viscous ellipsoidal inclusion in a slowly deforming matrix of contrasting viscosity

If both an inclusion and its matrix are incompressible and Newtonian viscous, then a homogeneous deformation of the inclusion and the resulting deformation in matrix is described by the following Eshelby's equations (Eshelby 1957, Bilby *et al.* 1975, Bilby & Kolbuszewski 1977, Freeman 1987):

$$\mu^M(\dot{\varepsilon}_{ij}^I - \dot{\varepsilon}_{ij}^M) = (\mu^M - \mu^I)S_{ijkl}\dot{\varepsilon}_{kl}^I \tag{A48}$$

$$\mu^M(\omega_{ij}^I - \omega_{ij}^M) = (\mu^M - \mu^I)\Pi_{ijkl}\omega_{kl}^I, \tag{A49}$$

where S_{ijkl} and Π_{ijkl} depend only on the instantaneous axial lengths of the inclusion. Their non-zero components are:

$$\begin{aligned}
S_{iiii} &= \frac{3}{8\pi}a_i^2 Ia_i a_i && (i = 1,2,3) \\
S_{iijj} &= \frac{3}{8\pi}a_j^2 Ia_i a_j && (i = 1,2,3; j = 1,2,3) \\
S_{ijij} &= \frac{3}{16\pi}(a_i^2 + a_j^2)Ia_i a_j && (i = 1,2,3; j = 1,2,3)
\end{aligned} \tag{A50}$$

$$\Pi_{ijij} = \frac{Ia_j - Ia_i}{8\pi} \qquad (i = 1,2,3; j = 1,2,3) \tag{A51}$$

with symmetrical relationships:

$$S_{ijij} = S_{ijji} = S_{jiij} = S_{jiji} \text{ and } \Pi_{ijij} = \Pi_{ijji} = -\Pi_{jiij} = -\Pi_{jiji},$$

where Ia_i and Ia_ia_j represent a set of integrals as follows:

$$\begin{aligned}
Ia_i &= 2\pi a_1 a_2 a_3 \int_0^\infty \frac{du}{(a_i^2 + u)\Delta} && (i = 1,2,3) \\
Ia_i a_i &= 2\pi a_1 a_2 a_3 \int_0^\infty \frac{du}{(a_i^2 + u)^2\Delta} && (i = 1,2,3)
\end{aligned} \tag{A52}$$

$$Ia_ia_j = \tfrac{4}{3}\pi a_1a_2a_3 \int_0^\infty \frac{du}{(a_i^2+u)(a_j^2+u)\Delta} \text{ (i = 1,2,3; } j = 1,2,3)$$

with:

$$\Delta = \{(a_1^2+u)(a_2^2+u)(a_3^2+u)\}^{1/2}.$$

Calculation of two-dimensional matrix strains

Consider a cylinder with unit-radius circular section embedded in matrix and deform the matrix by pure shear such that principal strain axes remain parallel to those of the ellipse section of the deformed cylinder. This is one of the cases discussed by Bilby *et al.* (1975). The deforming cylinder has axial lengths such that $a_1a_2 = 1$ and $a_3 \to \infty$. Because of pure shear, there is no vorticity, that is, $\omega_{ij}^I = \omega_{ij}^M = 0$. $\dot{\varepsilon}_{ij}$ can be diagonalized such that $\dot{\varepsilon}_{ij} = 0$ when $i \neq j$ and $\dot{\varepsilon}_{ii} = \dot{\varepsilon}_i$. Pure shear is then satisfied by $\dot{\varepsilon}_1 + \dot{\varepsilon}_2 = 0$ and $\dot{\varepsilon}_3 = 0$. Under these conditions Eshelby's equations (A48) and (A49) are simplified as follows:

$$\dot{\varepsilon}_1^M = \{1 + (r-1)(S_{1111} - S_{1122})\}\dot{\varepsilon}_1^I. \quad \text{(A53)}$$

Analytical solutions of S_{1111} and S_{1122} are given in Bilby *et al.* (1975) as:

$$S_{1111} = 1 - \frac{a_1^2}{(a_1+a_2)^2},\ S_{1122} = \frac{a_2^2}{(a_1+a_2)^2}.$$

Substituting these into (A53) and using $a_2 = 1/a_1$, we get:

$$\dot{\varepsilon}_1^M = \frac{(a_1^2+1)^2 + 2(r-1)a_1^2}{(a_1^2+1)^2}\dot{\varepsilon}_1^I. \quad \text{(A54)}$$

Integrating (A54) with the boundary condition that $a_1 = a_2 = 1$ when $t = 0$:

$$\varepsilon_1^M = \varepsilon_1^I + \tfrac{1}{2}(r-1)\tanh(\varepsilon_1^I) \quad \text{(A55)}$$

which is the solution given by Bilby *et al.* (1975). Equation (A55) can be rewritten in terms of strain ratio using $\varepsilon_1 = \ln R/2$:

$$\ln R^M = \ln R^I + (r-1)\tanh(\tfrac{1}{2}\ln R^I). \quad \text{(A56)}$$

This is the equation relating the strain ratio of matrix to that of the inclusion.

Calculation of three-dimensional matrix strains

Consider a sphere with unit radius embedded in matrix and deform the matrix by constant-volume coaxial deformation such that principal strain axes remain parallel to the ellipsoidal axes of the deformed sphere. This is one of the cases discussed by Freeman (1987). The deforming ellipsoid has axial lengths such that $a_1a_2a_3 = X^IY^IZ^I = 1$. Because of coaxial deformation, there is no vorticity and $\omega_{ij}^I = \omega_{ij}^M = 0$. $\dot{\varepsilon}_{ij}$ can be diagonalized such that $\dot{\varepsilon}_{ij} = 0$ when $i \neq j$ and $\dot{\varepsilon}_{ii} = \dot{\varepsilon}_i$. Constant-volume coaxial deformation is then satisfied by $\dot{\varepsilon}_1 + \dot{\varepsilon}_2 + \dot{\varepsilon}_3 = 0$. Under these conditions Eshelby's equations (A48) and (A49) are simplified as follows:

$$\dot{\varepsilon}_1^M = \dot{\varepsilon}_1^I + (r-1)(S_{1111} - S_{1133})\dot{\varepsilon}_1^I + (r-1)(S_{1122} - S_{1133})\dot{\varepsilon}_2^I \quad \text{(A57)}$$

$$\dot{\varepsilon}_2^M = \dot{\varepsilon}_2^I + (r-1)(S_{2211} - S_{2233})\dot{\varepsilon}_1^I + (r-1)(S_{2222} - S_{2233})\dot{\varepsilon}_2^I. \quad \text{(A58)}$$

Since $\varepsilon_1^I = \ln a_1$ and $\varepsilon_2^I = \ln a_2$, then $\dot{\varepsilon}_1^I = \dot{a}_1/a_1$ and $\dot{\varepsilon}_2^I = \dot{a}_2/a_2$. Substituting these into (A57) and (A58), we get:

$$\dot{\varepsilon}_1^M = \frac{\dot{a}_1}{a_1} + (r-1)(S_{1111} - S_{1133})\frac{\dot{a}_1}{a_1} + (r-1)(S_{1122} - S_{1133})\frac{\dot{a}_2}{a_2} \quad \text{(A59)}$$

$$\dot{\varepsilon}_2^M = \frac{\dot{a}_2}{a_2} + (r-1)(S_{2211} - S_{2233})\frac{\dot{a}_1}{a_1} + (r-1)(S_{2222} - S_{2233})\frac{\dot{a}_2}{a_2}. \quad \text{(A60)}$$

These two equations are solved numerically as done by Freeman (1987). While the right-hand sides of both (A59) and (A60) are numerically integrated with the boundary conditions that $a_1 = a_2 = a_3 = 1$ when $t = 0$, and that $a_1 = X^I$, $a_2 = Y^I$ and $a_3 = Z^I$ when $t = t$, the left-hand sides yield:

$$\varepsilon_1^M = \ln X^M \quad \text{(A61)}$$

$$\varepsilon_2^M = \ln Y^M, \quad \text{(A62)}$$

respectively. If the inclusion strain ellipsoid (X^I, Y^I and Z^I) is known, we can therefore numerically calculate the matrix strain ellipsoid (X^M, Y^M and Z^M).